The design of a brain and tumor phantom

Focused on mimicking the stiffness of the brain and glioblastoma multiforme tumor tissue

Master thesis by D.J. van der Molen

TUDelft

The design of a brain and tumor phantom

Focused on mimicking the stiffness of the brain and glioblastoma multiforme tumor tissue

by

D.J. van der Molen

to obtain the degree of Master of Science
at the Delft University of Technology,
to be defended publicly on Thursday July 8, 2021 at 10:00 AM.

This thesis is confidential and cannot be made public until July 8, 2023.

An electronic version of this thesis is available at `http://repository.tudelft.nl/`.

ŤUDelft

Preface

This report contains my master thesis concerning the design of a brain and tumor phantom, focused on mimicking the stiffness of the brain and glioblastoma multiforme tumor tissue. I did this project in partial fulfilment of the requirements for the degree of Master of Science in Biomedical Engineering at the Delft University of Technology.

My motivation for choosing Biomedical Engineering, with the track "Medical devices and Bioelectronics" at the TU Delft, was because of my interest for the technical aspects of the medical world. With this master thesis I hope I can contribute to the health and life quality of people through technology, which gives me the greatest satisfaction. This was my motivation for choosing the subject of my graduation project. This master thesis describes the project that was completed with the aim to develop a brain phantom with a glioblastoma multiforme tumor. The ultimate goal was to create this phantom with a similar stiffness compared to biological human brain tissue. I enjoyed the diversity of this project, such as the theoretical research, programming in Matlab and the practical work I had to do in the lab.

This thesis would not have been possible without the help of numerous people. Foremost, I would like to thank my supervisor, Dr. J.J. van den Dobbelsteen, for being an excellent mentor. He gave me guidance and more confidence in my work and truly clarifying feedback. Secondly, I would like to thank Ir. M. de Vries for his support and continuous advise during this master thesis project. I sincerely value both your continuous availability, your support and your believe in me, which greatly helped me to pursue this master thesis project. I would also like to thank J. van Frankhuyzen, who helped me with 3D printing and also during a very stressful moment when I was running out of time. Furthermore, I would like to thank Prof. Dr. B.H.W. Hendriks for taking the time to be part of my evaluation committee.

Also, I would like to thank F. Kor who inspired me to pursue this topic. Though his enthusiasm he impelled my interest and he motivated me to strive for the best possible outcome. Also, I would not have understood Rhinoceros so well without him. Furthermore, I would like to thank T. van den Brekel and C. Horsman who've always motivated and supported me.

Last but not least, I would like to thank my parents, brother and friends for their continuous support and for having faith in me. Hopefully, with this research I can make a small contribution to the overall goal.

D.J. van der Molen
Amsterdam, June 28, 2021

Summary

Glioblastoma multiforme tumors (GBM) are the most frequent and aggressive brain tumor type and have a very low survival rate. In order to improve the patient's outcome for a patient suffering from GBM the production of brain phantoms can be of great help. A brain phantom can be used for multiple purposes, such as neurological planning, training and for testing new medical devices. Nevertheless, no brain phantom has been created with realistic stiffness yet. Investigating the stiffness of the brain is challenging, due to the complexity of the brain and for not being able to touch it in person. However, through a relatively new technology called magnetic resonance elastography (MRE), it is possible to examine the stiffness of the brain. Hence, the objective for this thesis was to develop a brain phantom with a GBM tumor with similar stiffness compared to the biological human brain and tumor tissue.

In the literature MRE data can be found on the complex shear modulus of the brain and tumors, which can be converted to an indicative Young's modulus (E^*). The indicative Young's modulus will be used as a guideline for the desired stiffness needed for the production of a brain phantom. First various polyvinyl alcohol (PVA) samples were made and a compression test was carried out to derive the Young's modulus (E). By comparing E with E^*, it can be seen which PVA sample most resembles the brain and tumor tissue. Thereafter, the head phantom is created, which consists of 3 different production processes; production of the mould, production of the skull and production of the brain phantom. Firstly, the moulds for the brain phantom and tumor are 3D printed using polylactic acid (PLA). The skull phantom is derived from a patient specific CT scan, and is 3D printed with PLA. The brain phantom itself is made of 4,8 wt% PVA and 2 freeze-thaw (FT) cycles, and the tumor phantom is made of 5,2 wt% PVA and 1 FT cycle. The mass fractions and FT cycles have the closest stiffness compared to real brain and tumor tissue and were therefore selected. Within the brain phantom a hollow space is created where the tumor can be placed in. For a parallel project of the TU Delft and Utrecht University a brain phantom was required. For this specific case a brain phantom was produced with barium sulfate ($BaSO_4$), which functions as a contrast additive for CT and MRI. Therefore, the second brain phantom was made of 4,8 wt% PVA, 1 wt% BaSO4 and 2 FT cycles. The tumor phantom with $BaSO_4$ failed and therefore the first tumor without $BaSO_4$ was used for this use case. An experiment was carried out where a HoMS substance was injected into the tumor phantom. During the experiment 9 CT scans and 2 MRI scans were carried out. Due to the MRI and CT scans it could be investigated whether the tumor was in place and whether the brain phantom was visible in the CT and MRI. After the use case one more mechanical test was carried out consisting of PVA samples with $BaSO_4$ to examine whether $BaSO_4$ has an effect on the stiffness of the phantom.

The results of the mechanical test led to a desired mass fraction and FT cycle that can represent the brain and tumor phantom. These were immediately used for the production of the brain and tumor phantom. The Young's modulus of the brain phantom (E = 8,9 kPa) is a little stiffer compared to the actual brain tissue (E^* = 9,57 kPa). The Young's modulus of the tumor phantom (E = 5,8 kPa) is softer compared to the GBM tissue (E^* = 4,93 kPa). However, adding $BaSO_4$ to the PVA solution changed the stiffness of the PVA samples, has had an effect on the compactness of the samples, and the $BaSO_4$ did not dissolve properly. In the results of the CT and MRI scans it was found that the $BaSO_4$ was only visible in the inferior part of the brain. In addition, the brain and tumor phantom were clearly visible in the MRI and CT scans. It is therefore not recommended to use $BaSO_4$ for future research. Furthermore, the CT scan showed that the tumor phantom was well surrounded by the brain phantom and stayed in place even when the tumor was inserted by a cannula. The results show that a brain phantom with a tumor phantom can be produced. However, some improvements to the design of the mould are needed, because the mould was leaking, which subsequently led to an anatomically incorrect brain phantom.

This thesis project leads to the following conclusion; it is possible to produce a brain phantom with a GBM tumor phantom with comparable stiffness to the actual brain and GBM tissue. However, it can not be concluded that the various stiffness's are exactly the same as the actual brain and GBM tissue, but it is close to the values found in the literature.

Contents

List of Figures

List of Tables

List of abbreviations

|G*|	Shear stiffness
3mE	Mechanical, Maritime and Material Engineering
BaSO$_4$	Barium sulfate
CaCO$_3$	Calcium carbonate
CBTRUS	Central Brain Tumor Registry of the United States
CFS	Cerebrospinal fluid
CNS	Central nervous system
CT	Computed tomography
E	Young's modulus
E*	Indication Young's modulus
FDM	Fused Deposition Modeling
FFF	Fused Filament Fabrication
FT	Freeze-thaw
G'	Storage modulus
G"	Loss modulus
G*	Complex shear modulus
GBM	Glioblastoma multiforme
HoMS	Holmium microspheres
HoPLLAMS	Holmium loaded poly(L-lactic acid) microspheres
MISIT	Minimally Invasive Surgery and Interventional Techniques
MRE	Magnetic resonance elastography
MRI	Magnetic resonance imaging
PEEK	Polyether ether ketone
PLA	Polylactic acid
PMMA	Polymethylmethacrylaat
PVA	Polyvinyl alcohol
wt%	Mass fraction
ν	Poisson's ratio
μ	Shear modulus
φ	Phase angle

1

Introduction

The human brain is the most complex organ of the bodily and controls almost every body system [1]. Every year some 13.8 million neurosurgical cases evolve, of which 5% of the cases are brain tumors [2]. There are more than 120 different types of brain and central nervous system (CNS) tumors defined, of which the most common primary brain tumors are gliomas [3]. Gliomas account for 80% of all tumors arising in the brain tissue [4]. There are several types of gliomas, and the most frequent type is the glioblastima multiforme (GBM). Which is very aggressive and has a low survival rate [5]. A common treatment for these tumors is brachytherapy which is a minimally invasive technique [6].

It is important to improve the patients outcomes for patients who suffer from GBMs. In order to ensure this, both the treatment method and the necessary medical devices must be able to be continuously optimized, improved upon and further developed. A method that can be used for multiple medical purposes is using a brain phantom. This method has become more popular in recent years. A brain phantom is a 3D model mimicking tissue that stimulates the tissue properties in humans. For neurosurgeons a brain phantom could be desirable so that they can practice on a phantom instead of a cadaver. This is because the properties of the brain change post-mortem [7]. In addition, many studies have shown that surgeons trained with brain phantoms have superior skills in clinical procedures [8]. Furthermore, a brain phantom can be useful for the development of new medical devices. Because of this it can also be examined whether a new device functions properly. All in all a brain phantom can improve the training of neurosurgeons, decrease medical errors, and thus potentially improving patient outcomes and the development of new medical devices [7][9].

Depending on the purpose of the brain phantom, it must meet certain requirements for optimal use. One of the most important requirements is to mimic the mechanical properties of the brain. To possess knowledge about the mechanical properties of these tumors and the brain is of great importance to not only detect tumors but also to construct a realistic brain phantom. Although several studies have explored the mechanical properties of the brain and brain tumors, the mechanical properties of the brain are difficult to investigate because of the complexity of the brain and the complicated material it is composed of. Nevertheless, there are many different mechanical properties, but during this master thesis project the focus is on the stiffness of the brain [10].

In order to examine the stiffness of the brain and brain tumors, magnetic resonance elastography (MRE) can be used [11]. MRE is a non-invasive technique that makes it possible to investigate the stiffness of the brain. By means of the MRE data described in the literature values are found which represent the stiffness of the brain and tumors [12]. These stiffness values can be used as a guideline to reconstruct a brain phantom with a similar stiffness.

1.1. Problem statement

Although several brain phantoms have been produced in previous studies [13][14][15], a brain phantom with GBM tumor with a comparable stiffness to the biological brain tissue has not been produced yet. However, this would be of great interest in order to improve neurological training and testing new medical devices.

1

1.2. Objective
For this master thesis it was chosen to focus on the stiffness of the brain and GBM tumor and trying to mimic these. Therefore, the objective for this thesis can be defined as:

"The development of a brain phantom with a glioblastoma multiforme tumor with similar stiffness compared to biological human brain and tumor tissue"

1.3. Research questions
In order to examine whether the objective is obtained, three research questions have been formulated. The first research question is about whether it is possible to produce a brain phantom with a tumor phantom in it. The second research question is about the stiffness of brain phantom and whether that is similar to the stiffness found in the literature. The third research question is about the stiffness of the tumor phantom and whether that is similar to the GBM stiffness found in the literature. To answer these questions a compression test was carried out, and the head phantom was subjected to a computed tomography (CT) and magnetic resonance imaging (MRI) scan. The research questions are formulated as follows:

1. Is it possible to produce a brain phantom with GBM tumor phantom?

2. Is it possible to produce a brain phantom with a stiffness comparable to the stiffness found in the literature?

3. Is it possible to produce a GBM tumor phantom with a stiffness comparable to the stiffness found in the literature?

1.4. Thesis outline
To answer the research questions, and subsequently attain the objective, this master thesis is organized as follows: Chapter 2 provides a summary of the literature review that was done prior to this thesis project. This will provide information about the background and will summarize the literature on this thesis topic. Chapter 3 will describe the production process of the head phantom. Within this chapter the phantom requirements, determining of the stiffness and production of the mould, skull phantom and brain phantom will be elaborated upon. In chapter 4 a specific use case of a phantom will be described, using CT and MRI scans. Chapter 5 consists of an overall discussion of the results, describes the limitations of this thesis and gives recommendations for future research. Finally, chapter 6 provides the reader with the conclusion of this master thesis and gives answers to the research questions.

<div style="text-align: right; font-size: 4em;">2</div>

Background and literature

The goal of this chapter is to provide background information important to this thesis project. A lot of information originates from the literature study that was performed prior to this master thesis. Only the essential and relevant parts of the literature study are included and some new literature was added. For additional information this literature study can be consulted [16].

2.1. Anatomy and physiology

The human brain plays a role in almost every bodily system and it has many essential functions. Some of these functions include the processing of sensory information, the control of breathing, the release of hormones and the regulation of blood pressure. The brain can be divided into three main parts; the cerebrum, cerebellum and the brain stem, see Figure 2.1.

2.1.1. Cerebrum

The cerebrum is the superior part of the brain and composes 83% of the total brain mass. It consists of a right and left cerebral hemisphere, whereby each hemisphere controls the opposite side of the human body. The two hemispheres are incompletely separated by the longitudinal cerebral fissure, which is a deep median groove. The longitudinal cerebral fissure of the cerebrum contains the dura mater and the anterior cerebral vessels. Through the corpus callosum the two hemispheres connect across the median plane.

The cerebrum can also be divided into functional lobes through the hemispheres and have separated fissures. Each hemisphere contains five lobes; frontal, temporal, parietal, occipital and insula (located deep inside the brain), see Figure 2.2. These lobes can be divided again into areas that play very specific roles. The most essential functions of the cerebrum are; interpreting touch, vision, hearing, control of speech, reasoning, emotions, learning and control of movement [1].
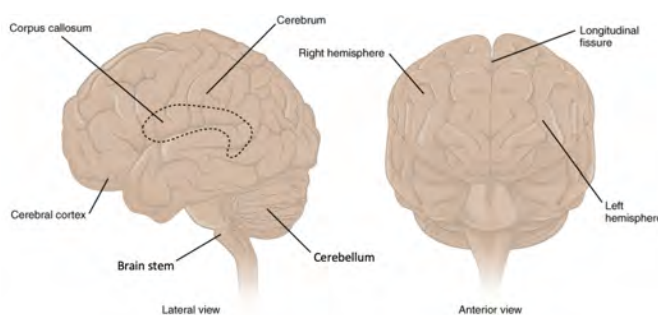
Figure 2.1: The cerebrum, cerebellum and brain stem [17]   **Figure 2.2:** Lobes of the cerebral cortex [17]
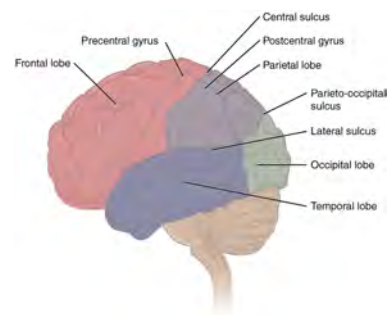
The cerebrum consists of two parts: the gray and white matter. The gray matter is the cerebral cortex of the brain and is a folded sheet with a thickness ranging from 1.0 to 4.5 mm, with an overall average of 2.5 mm [18][19]. Primarily, the gray matter consists of neuronal cell bodies, protoplasmic astrocytes and microglia.

The cortex is a folded structure, which has the function to increase the surface of the brain. Each fold is called a gyrus and each groove between the folds is called a sulcus [20]. The white matter is the interior brain tissue and contains oligodendrocytes, which wrap a myelin sheath around the axons, fibrous astrocytes and microglia [18][21]. The whitish color is because of the relatively high lipid fat content of the myelin protein [21]. The axons in the white matter connect distant neurons in the cortical gray matter [22].
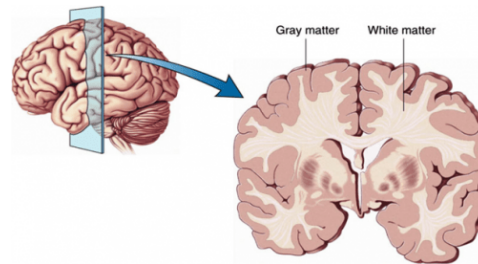
Figure 2.3: Frontal section of the gray and white matter of the brain [23]

2.1.2. Cerebellum

The cerebellum accounts for 11% of the total brain mass and is located under the cerebrum. The two cerebellum hemispheres are medially connected by the vermis. Comparable to the cerebrum, the cerebellum consists of an outer cortex of gray matter and of internal white matter [24]. The cerebellum is mainly responsible for coordinating muscle movements and maintaining posture and balance [1].

2.1.3. Brain stem

The brain stem only accounts for 2.5% of the total brain mass and connects the cerebrum and cerebellum with the spinal cord. The histology of the brain stem is almost similar to the spinal cord with deep gray matter surrounded by white matter fiber tracts [24]. The brain stem is mostly responsible for the automatic functions which include; breathing, heart rate, body temperature, wake and sleep cycles, digestion, sneezing, coughing, vomiting and swallowing [1].

2.1.4. Blood supply

The four arteries responsible for the blood supply to the head and neck are the common carotid arteries, the vertebral arteries, the thyrocervical trunks and the costocervical trunks. The common carotid arteries split up into an internal and external branch. Blood is supplied to most tissues of the head by the external carotid arteries. The internal carotid arteries enter the skull through the carotid canals of the temporal bones and supply more than 80% of the blood to the cerebrum. In addition, the internal carotid arteries also supply blood to the orbits, eyes, forehead and nose. The vertebral arteries supply the cerebellum, brain stem and the underside of the cerebrum [24]. The vertebral arteries stem from the root of the neck and enter the brain through the foramen magnum of the occipital bone. Figure 2.4 illustrates the arteries in the brain. This structure is called the circle of Willis [17].
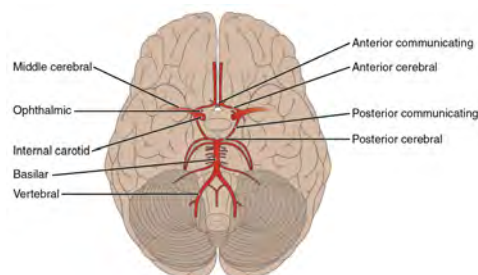
Figure 2.4: Inferior view of the arteries in the brain [17]

2.1.5. The cranium

The cranium (skull) is the most complex bony structure of the human body and has the function of protecting the face and brain from injury. The skull consists of cranial and facial bones [24]. The facial bones support the facial structures and the cranial bones form the brain case, which is also called the cranial vault. This brain case surrounds and protects the brain and is furthermore responsible for the housing of the internal ear [17]. The cranial vault consists of eight cranial bones; the paired parietal and temporal, and the unpaired frontal, the sphenoid, the occipital and the ethmoid [1].

The interior space of the cranial vault is called the cranial cavity and houses the brain, its meninges, and their blood vessels. The internal surface of the base of the skull has a complex structure and has diverse cavities for the passage of cranial nerves, blood vessels and the spinal cord. The base can be subdivided into three parts; the anterior cranial fossa, the middle cranial fossa and the posterior cranial fossa [17].
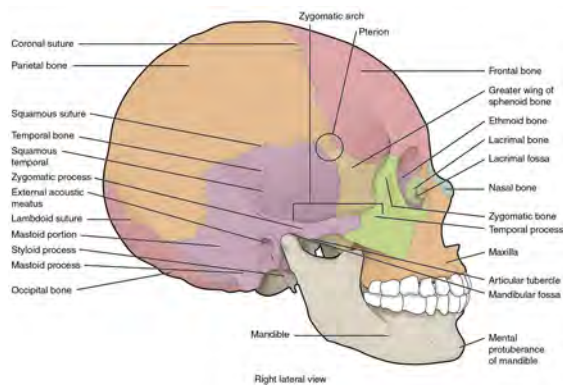
Figure 2.5: Lateral view of the cranium [17]
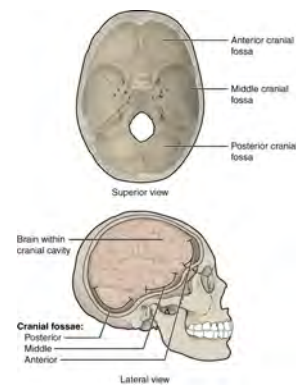
Figure 2.6: Superior and lateral view of the cranial fossae [17]

2.1.6. Meninges

Meninges are three different layers composed of connective tissue; the cerebral dura mater, the arachnoid mater and the pia mater. The meninges are located between the outer layer of the brain and the inner surface of the cranium [17]. The cerebral dura mater lines in the interior cranial vault and consist of two layers, an inner and an outer layer. The dura mater serves two functions: 1) membrane support for the brain and 2) an internal periosteum to the bones. The structure is mostly fibrous, consisting of white collagen fibers with an alloy of elastic fibers. The arachnoid mater is the intermediate layer of the meninges. The subdural space separates the dura mater from the arachnoid mater. Furthermore, the arachnoid mater is separated from the pia mater by the subarachnoid space, which is filled with cerebrospinal fluid (CSF) [1]. CSF serves as a liquid cushion for the brain. The pia mater is the layer covering the entire surface of the brain, including in the cerebral gyri and between the cerebellar laminae. It is a thin fibrous membrane and has a continuous layer of cells providing a fluid-permeable membrane [1][17].

2.2. Imaging techniques

For pre-operation diagnostics and image registration patient-specific data is needed, which can be extracted from radiological images such as CT and MRI scans [25]. CT and MRI are the most common imaging techniques and can help the surgeon to detect, localize and evaluate brain tumors [26][27].

2.2.1. Computed Tomography

CT is a x-ray procedure that generates cross-sectional images of the body. By absorbing various amounts of x-rays in different tissue types a detailed contrasted image is made. These cross-sectional images are called tomographic images and form a three-dimensional image. The 3D image provides information about the anatomy and detect possible tumors or abnormalities in the tissue [28][29]. The use of CT scans can be very advantageous, since it has a high availability and can be quickly implemented by the surgeon. However, ionizing radiation is produced by x-rays which can cause damaging biological effects in living tissue, such as developing solid organ cancers and leukemia [30].

2.2.2. Magnetic Resonance Imaging

MRI produces a three dimensional image of the body using a magnetic field and radiofrequency current. MRI can generate high resolution images with great soft tissue contrast, and can be used to identify lesions in the brain or spinal cord. Furthermore, MRI has the benefit, contrary to CT, of not producing ionizing radiation. This is an advantage and therefore MRI is vastly superior and thus preferred as an imaging technique [31][32]. A MRI scan can be performed with different MRI sequences, whereby the most common ones are the T_1-weighted and T_2-weighted scans. T_1-weighted is generated with short relaxation and excitation time and T_2-weighted is generated with long relaxation and excitation time. By changing the parameters of the MRI scanner, the contrast of the MRI can change [33].

2.2.3. Magnetic Resonance Elastography

MRI an CT have not only been used as imaging techniques, but also to determine the stiffness of brain tumors. Nevertheless, the results of these techniques reported in studies have been inconclusive or inconsistent. Therefore, using MRE is a more adequate technique to estimate the stiffness of tissue and thereby detecting tumors. This technique is useful for parts in the body that are not accessible to the physicians hand, such as the human brain [11][10]. MRE is an MRI based imaging technique used to image small amplitude vibrations within the brain. This is created by transmitting mechanical vibrations to the skull with a frequency between 15 - 100 Hz [32][11].

MRE allows virtual "palpation" and thereby makes it possible to investigate the mechanical properties of the brain non-invasively [12]. The relation between the shear modulus and the elasticity modulus is defined by formula 2.1. The G' is the storage modulus, also known as the shear stiffness or elasticity modulus, and G" is the loss modulus, also known as the shear viscosity [34][11]. Due to the storage modulus the amount of structure present in a material can be defined and represents the energy stored in the elastic structure. Furthermore, the loss modulus describes the amount of energy dissipated in the brain structure. Using the G' and G", the phase angle φ and complex shear modulus G^*, can be calculated. The complex dynamic shear modulus is the 'sum' of the loss and storage modulus, see formula2.1 [35]. The complex shear modulus represents the unit stress response to a unit shear strain [32]. The shear stiffness $|G^*|$ can be described as the magnitude of the complex shear modulus and quantifies the amount of storage and loss properties, see formula 2.2 [36][37]. The phase angle φ can be used as a measure for the ratio between the G' and G", see formula 2.3. See Figure 2.7, whereby the relation between the components G' and G", the phase angle φ and the G^* are represented. It can be seen from the figure below that a small phase angle φ means a lower viscosity compared to the stiffness, and vice versa [11].

$$G^* = G' + iG'' \tag{2.1}$$

$$|G^*| = \sqrt{G'^2 + G''^2} \tag{2.2}$$

$$tan\varphi = \frac{G''}{G'} \tag{2.3}$$

Figure 2.7: The relation between G', G", G^* and the phase angle φ [11]

2.3. Neurological diseases

Approximately 13.8 million crucial neurosurgical cases evolve each year. Table 2.1 lists the estimated number of cases requiring neurological operation worldwide. Whereby 5% of the neurological cases are caused by brain tumors, about 735.180 cases annually [2].

2.3.1. Tumors

A brain tumor is an abnormal mass of tissue in which cells grow and multiply uncontrollably [38]. There are more than 120 different types of brain and central nervous system tumors, which can be identified by the classification system of the World Health Organization [3].

Neurological cases	Cases per year	Proportion per year (%)
Traumatic brain injury	6.160.814	44,7
Stroke	2.760.403	20,0
Epilepsy	1.413.426	10,3
Hydrocephalus	971.317	7,0
Infections	969.001	7,0
Brain tumor	735.180	5,3
Traumatic spinal injury	399.606	2,9
Vascular Anomalies	311.407	2,3
Neural tube defect	35.622	0,3
Spinal tumor	17.840	0,1
Total	13.786.823	

Table 2.1: Number of neurological cases requiring neurological operation worldwide [2]

Most brain tumors can be divided into two main groups; primary and metastatic tumors. Primary tumors include tumors that emerge from the brain or the surrounding tissue. The primary tumors can be categorized as being benign or malignant. Benign tumors grow slowly and do not intend to spread. In contrast, malignant tumors grow more rapidly and frequently spread to surrounding tissues [38].
Metastatic brain tumors, known as secondary brain tumors, include tumors that primary stem from another location in the body and spread to the brain. Approximately 20% to 40% of adult cancer patients suffer from metastatic brain tumors [39]. Metastatic tumors are considered as cancer and as malignant [38]. Comparing the annual incidence of metastatic and primary brain tumors, it was declared that these affect 2.8 and 7.8 persons per 100.000 population respectively [40][41][42].

2.3.2. List of common brain tumors
The distribution of histologic diagnoses of primary brain tumors and CNS tumors registered by the Central Brain Tumor Registry of the United States (CBTRUS), is illustrated in Table 2.2. The meningiomas are the most common benign brain tumors and occur in 30.1% of the cases. Glioblastomas are the most common malignant brain tumors and have an occurrence of 20.3% [43].

Histology	Percentage (%)
Lymphoma	3.1
Nerve sheath	8.0
Craniopharyngioma	0.7
Pituitary	6.3
Glioblastoma	20.3
Astrocytomas	9.8
Ependymomas	2.3
Oligodendrogliomas	3.7
Embryonal, including medulloblastoma	1.7
Meningioma	30.1
All other	13.9

Table 2.2: Number of all primary brain and CNS tumors registered by the CBTRUS [43]

2.3.3. Gliomas
The most common primary brain tumors are the gliomas, which account for 80% of all tumors arising in brain tissue [4]. Gliomas have a high mortality rate, with an average survival rate of 12-15 months for GBMs, and 2-5 years for low grade gliomas [37]. GBMs respond badly to treatment and have a high recurrence rate outcome, which leads to a low survival rate for the patient [5]. Gliomas originate from the supporting structures of the brain and vary in size, location, clinical behavior and histological structure [44]. The neurological symptoms differ per patient but can include headaches, seizures, focal neurologic deficits, memory loss, personality changes, vomiting, and visual changes.

The malignancy grade of the gliomas can be ranked from I - IV, comparable with other tumors, whereby grade I is a low grade glioma and grade IV is a high grade glioma, which is called the GBM [4]. There are ten types of gliomas of which the astrocytoma, oligodendroglioma, ependymoma and GBM are the four most frequent ones, see Table 2.3 [44][43]. GBM is the most common type and accounts for the most aggressive primary tumor in adults, with an incidence of 50.7% [43]. Its cells multiply rapidly, irregularly, and originate from the cerebral white matter [44]. Most gliomas, 86%, occur in the cerebral hemispheres, varying in location in the brain, which is shown in Table 2.4 [45].

Histology	Percentage (%)
Ependymomas	5.6
Oligodendrogliomas	9.2
Pilocytic astrocytomas	5.7
Diffuse astrocytomas	1.7
Anaplastic astrocytomas	7.9
All other astrocytomas	9.1
Glioblastomas	50.7
All other gliomas	10.1

Table 2.3: Number of primary brain tumors and CNS gliomas registered by the CBTRUS [43]

Location in the brain	Percentage (%)
Frontal lobe	40
Temporal lobe	29
Parietal lobe	14
Occipital lobe	3
Deep cerebrum	6.4
Ventricles	2.2
Cerebellum	1.5
Brain stem	4.1

Table 2.4: Number of the locations of the gliomas in the brain regions [45]

2.4. Mechanical properties

The mechanical properties of the brain are difficult to investigate because of the complexity of the brain and the complicated material is is composed of. The brain tissue is more or less heterogeneous on macro- and microscale. Furthermore, the geometry of the brain tissue is complex [46].

2.4.1. Gray and white matter

The mechanical properties of the brain appear to vary between the gray and white matter. Numerous researches have been done to investigate the stiffness, and the viscoelastic properties, of the gray and white matter of the brain. In Table 2.5 is shown that white matter is more viscous and stiffer than gray matter. Because white tissue consists of oriented nerve fibers, white matter is considered to be anisotropic while gray matter is nearly isotropic [18]. According to Mota *et al.* the maximum stress of white matter is 20% higher than that of gray matter, at the highest strain rate [22].

Region	Tissue type	G'(kPa)	G"(kPa)
Cerebellum	Gray matter	1.77 ± 0.24	0.94 ± 0.17
	White matter	1.85 ± 0.18	1.10 ± 0.23
Cerebrum	Gray matter	2.34 ± 0.22	1.11 ± 0.03
	White matter	2.41 ± 0.23	1.21 ± 0.21

Table 2.5: Storage- and loss modulus in the two different brain regions, at 80 Hz (mean ± SD) [34]

2.4.2. Cerebrum and cerebellum

The mechanical properties of the cerebellum and cerebrum differ. In Table 2.5 the mean and standard deviation of the storage- and loss modulus are shown regarding the white and gray matter in the cerebrum and cerebellum. The cerebellum is (23-24%) softer than the cerebral hemispheres. However Zhang *et al.* state that there is no difference in viscosity between the two brain regions. In addition, the number of glial cells is lower in the cerebellum than in the cerebrum, and therefore cells may be less tightly bound together [34].

2.4.3. Factors influencing mechanical properties

Several factors can have an effect on the mechanical properties of the brain. For instance, the stiffness of the brain is affected due to the large number of blood vessels in the brain. These blood vessels give more firmness to the soft brain tissue when these are under pressure [46]. In addition, the mechanical brain tissue

properties in extension differ from those in compression. The behavior of the tissue differs during a surgical procedure when compared to normal circumstances [47].

2.4.4. Gliomas

A MRE measurement, at a frequency of 60 Hz, was performed to analyse the shear stiffness of different grade gliomas, as shown in Figure 2.6. According to the research of Pepin *et al.* there is a negative correlation between the glioma grade and the magnitude $|G^*|$, whereby the stiffness decreases when the glioma grade increases. Furthermore, gliomas demonstrate softer characteristics than healthy brain tissue does. In addition, they reported a relatively lower stiffness in metastatic GBMs as compared to primary GBMs [11][37].

	$|G^*|$ (kPa)
Healthy white matter	3,3 ± 0,7
Glioma grade II	2,7 ± 0,7
Glioma grade III	2,2 ± 0,6
Glioma grade IV	1,7 ± 0,5
Mean stiffness	2,2 ± 0,7

Table 2.6: comparing the shear stiffness of different grade gliomas [37]

2.5. Treatment for GBMs

GBMs can occur in any part of the brain, such as the cerebellum, brainstem and cerebrum. However a GBM mostly occurs in the cerebrum in the frontal and temporal lobe. These tumors tend to invade surrounding brain tissue and thus cannot be removed completely by a resection using craniotomy. In addition, these do not respond well to chemotherapy or radiotherapy. However, radiotherapy is the most effective treatment and offers temporary relief, but this treatment can affect the surrounding healthy tissue. In order to reduce the side effects of radiotherapy, the radiation needs to be localized in the target area of the tumor [6]. Therefore, brachytherapy can be used as a minimally invasive technique. This treatment consists of neuro-navigated needle injections of a radioisotope, with a weak penetration power, into the tumor using CT or MRI [48]. M. de Vries developed an administration device for the brachytherapy treatment of brain tumors. This device uses radioactive holmium microspheres (HoMS) as radioisotope and consists of two parts. The cannula, which is a hollow needle is used for guidance trough the brain, and the steerable pre-bend stylet inside the cannula, through which the HoMS will be injected [49]. Figure 2.8 illustrates the cannula that punctures the tumor tissue. In Figure 2.9 the injection of the radioisotope, though the pre-bend steerable stylet is shown. Due to this treatment technique the radiation dose in the tumor can be higher than conventional radiation, without damaging the healthy surrounding tissues [48].
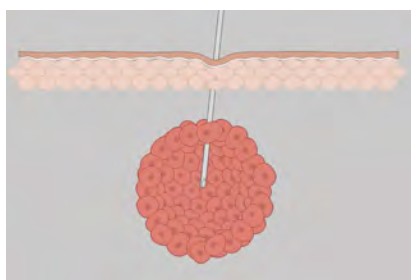
Figure 2.8: The cannula in the tumor tissue [48]
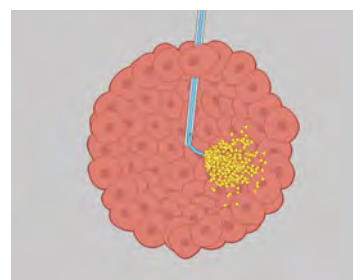
Figure 2.9: The injection of the radioisotope in the tumor tissue [48]

2.6. Phantom characteristics

The goal of this section is to address what is known of brain phantoms as well as to discuss the necessities for the production of a brain phantom. Firstly, some general information about brain phantoms will be provided. Secondly, the material needed for the brain phantom will be described. Thirdly, the casting process will be explained, after which the 3D printing technique used will be elaborated upon. Lastly, contrast additives will be discussed for MRI and CT.

2.6.1. Brain phantoms

Brain phantoms are useful for experimental studies, due to the complex brain tissue properties. Brain properties have different properties in vivo than in vitro, and the mechanical properties change rapidly post-mortem. Therefore, it would be advantageous to replace the soft brain tissue with brain phantoms for experimental studies. The benefits of a phantom are that these are more controllable, easier to handle and that these eliminate the problem of sample-specific variations. Because of these benefits, brain phantoms can be utilized in numerous fields, ranging from surgical training to the modeling of interactions between soft tissue and medical tools, for instance the validation of needle insertions or demonstrate new needle concepts [50][51][52]. An important characteristic of a brain phantom is that it should closely mimic the relevant properties of the brain tissue [7].

2.6.2. Polyvinyl alcohol

Many studies have been done on materials that are useful for brain phantoms. However, a large variety of materials, with a broad range of material properties, exist [52]. Most tissue-mimicking materials have been made using an agar or gelatin base [53]. However, polyvinyl alcohol (PVA) has recently become a popular material for tissue engineering, because it is a hydrophilic, biodegradable and biocompatible synthetic polymer. Further PVA is used for tissue-mimicking phantoms because the mechanical properties of soft tissue can be easily mimicked. PVA hydrogels are water-swollen, cross-linked, polymer networks [54]. When a PVA solution undergoes a period of freezing and is then allowed to thaw to at room temperature, this is called a freeze-thaw (FT) cycle. FT cycles transform the liquid PVA solution into an elastic gel [55]. By increasing the number of FT cycles, the structure of the PVA hydrogel can change. When the FT cycles are increased, the cross-links increase, and therefore the stiffness of the PVA phantom increases [53]. PVA is a good material for the production of a brain phantom because of its similar texture and its mechanical properties, such as compressibility and elasticity [55].

2.6.3. Casting process

The casting technique is a commonly used method for the production of a brain phantom, due to its low cost and its ability to create simple structures. Using this technique, a mould is made of a negative 3D image, which is then filled with a liquid material. The liquid material adapts to the shape of the inside of the mould and hardens. The production of the mould can be done in a broad variability, depending on the type of casting technique. An important aspect of the mould production is that multiple layers are applied over a plastic brain model [56]. Although the casting technique is a commonly used method, another technique has come to light. A mould can nowadays be printed using 3D printing.

2.6.4. 3D Printing

In recent years 3D printing has become increasingly popular. This technique can be used to print implantable prostheses, print tissue biomimetically, or can be used to develop moulds for tissue engineering. The advantage of 3D printing is the ability to create a mould containing patient-specific structures. Compared to the casting technique the mould can be printed directly, which makes this technique faster. In addition, 3D printing is a relative affordable technique. Due to the increased popularity of 3D printing many less expensive 3D printers are being developed. These 3D printers are using the Fused Deposition Modeling (FDM) technology, also known as Fused Filament Fabrication (FFF). FDM deposits heated material by extruding it through a nozzle, whilst moving around the build plate, see Figure 2.10. The print head moves horizontally, layer by layer, while the build plate moves vertically. The print head of FDM has two nozzles; one for the build material of which the model will be made of, and one for the support material for the support of the complex structures of the model. The build material, polylactic acid (PLA), is a commonly used material because of its benefits, such as its rapid printing speed, its low melting point, its easy availability and being low in cost. PVA is a frequently used support material because of its water solubility, and can therefore be easily removed [57]. For all of the advantageous reasons mentioned above, 3D printing will be a great technique for the production of a head phantom, and not only for the production of moulds but also for the production of the skull, which will be further elaborated upon in section 3.4.1.
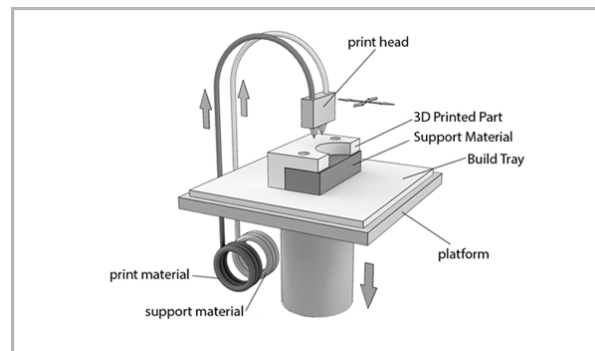
Figure 2.10: FDM technology [58]

2.6.5. Contrast additives

For the creation of a phantom, contrast additives are required to create the contrast for CT and MRI scans. This is because not all tissue mimicking materials are visible in the CT and MRI scans, or do not have the same comparable contrast as human tissue does. Consequently, the additives for the brain phantom need to be mixed with the base material (PVA) in order to create sufficient contrast. To increase the contrast of a PVA phantom in a CT scan, powdered barium sulfate ($BaSO_4$) is a commonly used material. When preparing the PVA solution with 1 wt% to 2 wt% of $BaSO_4$ the phantom will show enough contrast in the CT [55]. Another method to make parts of the phantom visible in a CT scan is by adding markers as a referential point during the CT [59]. For the contrast for in a MRI scan $BaSO_4$ has no effect, unless more than 60 wt% is used in the PVA mixture. However, PVA phantoms are already visible in MRI scans, thus contrast additives are not needed [53]. Not only must the brain phantom show contrast during CT and MRI scans, but the skull needs to show this too. Using PLA, with calcium carbonate ($CaCO_3$) powder particles in it, as a build material for 3D printing can improve the CT contrast. However, this does not apply to MRI [15].

3

Production of the head phantom

The goal of this chapter is to describe the production process of the phantom. Firstly, the requirements of the phantom will be discussed. Secondly, different PVA samples were created, and a compression test was carried out. Using the compression test data, the desired PVA concentration of the samples was determined by comparing these to the literature data on real brain and GBM tissue. Then the production process of the head phantom will be discussed. The production of the head phantom is divided into three sections; the production of the mould, the production of the skull and the production of the brain phantom.

Research by F. Kor

In 2019 F. Kor made a head phantom. In his thesis report some limitations were described and recommendations for future research were given. These recommendations can be used to improve a head phantom. However, the focus of this thesis differs from the thesis of F. Kor, and therefore not all limitations and recommendations can be used.

In the thesis of F. Kor 10 neurosurgeons completed a questionnaire about head phantoms. The questionnaire results showed that the mechanical properties of the brain phantom did not match the real brain. Therefore, F. Kor recommended to improve these mechanical properties. This recommendation is relevant as this thesis is focused on the stiffness of the brain phantom. In order to improve the stiffness, research needs to be done on the on the stiffness of the brain, and tumor tissue and in matching tissue mimicking materials, first. According to F. Kor, the 6 wt% PVA of the brain phantom did not match with real brain tissue [13]. Therefore, an experiment is carried out in section 3.2 to compare different PVA concentrations, with different FT cycles. The results of this experiment will give an overview on which PVA concentration is desired to match the stiffness found in the literature as closely as possible.

3.1. Phantom requirements

The first two requirements are the most important ones. The brain and tumor phantom need to have stiffness as close as possible compared to the actual brain and GBMs. This will help the phantom to be as realistic as possible. This is especially important for neurological training and the development of new medical devices, where the neurosurgeons can practice with operating in the brain phantom, getting a realistic feedback. Thirdly, the material used for the phantom needs to have easily controllable mechanical properties, in order to meet the right stiffness requirement. In addition, the manufacturing of phantoms must be inexpensive and easy. Furthermore, there should not be a displacement of the tumor phantom in the brain, during the production process, or when the phantom will be used. Lastly, the phantom needs to have enough contrast to be seen by a CT and MRI scan.

The list of requirements:

1. The stiffness of the brain phantom must be close to real brain

2. The stiffness of the tumor phantom must be close to GBMs

3. Materials with easily controllable mechanical properties should be used

4. Easy and inexpensive to manufacture

5. No displacement of the tumor phantom in the brain during the production process

6. Contrast for CT/MRI

3.1.1. Meeting the requirements
In order to produce the head phantom, and meet all requirements, an incremental process will be used, whereby the production process will be split into research phases, thus determining the desired stiffness, as well as creating the head phantom and a use case for using the head phantom with CT and MRI.

1. The first research phase is to examine stiffness of different PVA samples, and determine the desired PVA concentration (section 3.2). During this phase it will be examined whether the samples meet requirements 1 - 3.

2. The second research phase is to develop the head phantom with the tumor (section 3.3, 3.4 and 3.5). Whereby the phantom needs to meet the requirements 1 - 5.

3. The last research phase is to develop a head phantom for a specific use case (chapter 4). The phantom will thus be evaluated by seeing whether all requirements (1 - 6) are met.

3.2. Determining the stiffness
The goal of this section is to determine the desired PVA concentration, a concentration that has the most realistic mechanical properties compared to brain and tumor tissue. As mentioned in section 2.6.2, PVA is a suitable material to use for creating a brain phantom. However, there is a lack of information concerning the correlation between the concentration of PVA, number of FT cycles and its mechanical properties. For this purpose, different PVA samples with various stiffnesses were created. Subsequently, a compression test was carried out to determine the stress-strain curve. The Young's modulus (E) can be derived from the slope of the stress-strain curve. The stiffness of the human brain and tumor is established in the literature with a dynamic test. This dynamic test is performed with a MRE, which provides the complex shear modulus (G^*). By combining the two variables E and G^* an estimated concentration of PVA can be described.

3.2.1. Method of production
Production of the PVA samples
Firstly, different PVA solutions were made with varying mass fraction (wt%) of the PVA powder, whereby 5 different sample groups were created. Each sample group consists of 3 samples with the same wt% PVA.
To prepare the PVA, the technique used by Chen *et al.* is applied [55]. For an elaborated version of the preparation of PVA see Appendix B. As well as Chen *et al.*, the research of F. Kor created a brain phantom with a 6 wt% PVA and was subjected to 1 FT cycle. Since GBM is a softer tissue compared to brain tissue, the samples groups created in this experiment have a lower PVA wt% compared to these previous experiments. Also different FT cycles were applied. The PVA powder dissolves in a distilled water and coolant mixture, whereby the coolant prevents the mould from breaking due to expansion during freezing. The specific PVA that is used for the samples is the polyvinyl Alcohol 99+% hydrolyzed (SIGMA-ALDRICH, USA), the distilled water (C+V Pharma-Depot GmbH, Germany) and the coolant liquid type D/G12 (Carsprint, Belgium). Table 3.1 shows the composition of the materials, mass fraction and the number of FT cycles.

Sample group	Water (g)	Coolant (g)	PVA (g)	wt% PVA	FT cycle
1	80	20	4,5	4,3	2
2	80	20	5,0	4,8	2
3	80	20	5,0	4,8	1
4	80	20	5,5	5,2	1
5	80	20	6,5	5,7	1
Note. 3 equal samples are made from each sample group					

Table 3.1: Proportions that are required to make the four PVA samples groups

Mechanical test

The stiffness of the PVA samples will be compared to the stiffness of the brain and tumor found in the literature. Therefore a mechanical test will be carried out to generate a stress-strain curve and calculate E. An uniaxial compression test was performed using a linear stage PRO-115-400-UF (Aerotech, USA/UK). The linear stage is located in the Minimally Invasive Surgery and Interventional Techniques (MISIT) laboratory at 3mE, TU Delft. The force was measured with a 22 N Force Sensor, LSB200 (FUTEK, USA). The force sensor is mounted between the linear stage and a square surface, with an area of 1600 mm^2. The PVA samples were compressed by the square surface on the linear stage. The linear stage was set-up using a strain of 30%, and a compression speed of 1 mm/s. On each sample a measurement was performed, which resulted in a total of 3 measurements per sample group. All the tests were carried out at room temperature. Figure 3.1 shows the experimental set-up of the compression test.
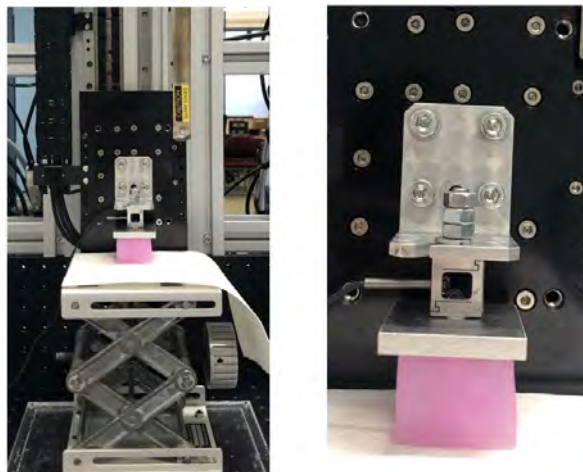
Figure 3.1: The experimental set-up of the linear stage with the force sensor and the PVA sample

The raw data of the compression test consisted of a measured output voltage, speed and position. By calibrating the force sensor, the output voltage was converted to a measured force. Using this force, the stress and strain were calculated in MATLAB, and a stress-strain curve was created. To remove the noise in the stress-strain curve a moving average was used to create a clearer line.

Indicative Young's modulus

The compression test that was carried out on the PVA samples was a quasi-static test which resulted in the E. The literature has shown that the mechanical properties of the brain and tumor can be measured by MRE. MRE is a dynamic test and the complex shear modulus (G*) can be derived from it. In order to compare the quasi-static test with the dynamic test, a relation between the E and G* must be described. According to Morin *et al.* there is a relation between the shear modulus and the Young's modulus, see equation 3.1, whereby the complex shear modulus is used as the shear modulus (μ). Morin *et al.* used a Poisson's ratio (v) of 0.45 as the brain tissue is a quasi incompressible. In addition, the indicative Young's modulus (E*) can be computed. It must be taken into account that the indicative Young's modulus calculated by equation 3.1 can only be used as an indication [60].

$$E^* = 2\mu(1 + v) \tag{3.1}$$

The study by Pepin *et al.* performed a MRE to determine the magnitude of the shear modulus of the healthy white brain tissue and different types of gliomas (Table 2.6, subsection 2.4.4) [37]. These values will be used as the normal shear modulus to calculate the E*, using equation 3.1 to obtain the range values of the indicative Young's modulus for this thesis project.

3.2.2. Results

Figure 3.2 shows one of the square PVA samples. The dimensions of the PVA sample are the following: 3,3 ×
3,3 × 3,3 cm.

Figure 3.2: A PVA sample with the dimensions 3,3 × 3,3 × 3,3 cm

Figure 3.3 illustrates 5 different stress-strain curves, one curve for each sample group. There one curve is the
average of the 3 measurements that were carried out on a sample group. The blue line is sample group 1, red
is sample group 2, green is sample group 3, black is sample group 4 and pink is sample group 5. The curves
are a non-linear line, which demonstrate that the PVA samples are composed of a viscoelastic material. See
Appendix A for more stress-strain curves of the samples.
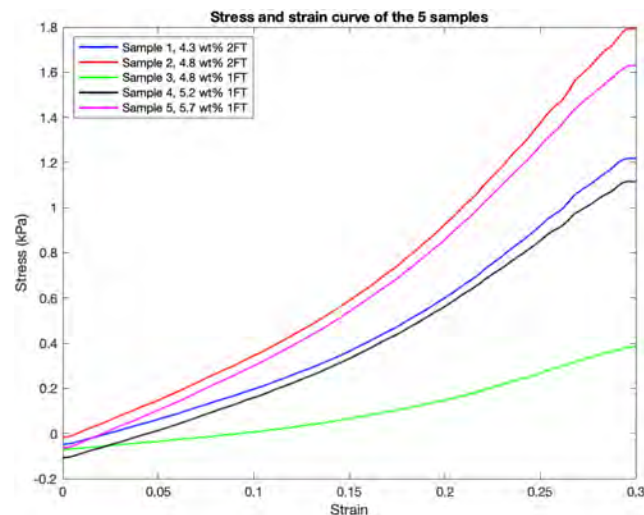
Figure 3.3: The average stress strain curves of the 5 different sample groups. Blue: Sample group 1 (4.3 wt% PVA, 2 FT). Red: Sample
group 2 (4.8 wt%, 2 FT). Green: Sample group 3 (4.8 wt%, 1 FT). Black: Sample group 4 (5.2 wt% PVA, 1 FT). Pink: Sample group 5 (5.7
wt% PVA, 1 FT)

Subsequently, the Young's modulus was derived from the slope of the stress-strain curve between the strain
of 19% - 29%. The PVA samples do not have a perfectly initial shape, caused by a partial pressure on the
sample before the compression test started. Therefore, the lower stress and strain values are less reliable
when compared to the higher stress strain. Table 3.2 shows the range of Young's modulus values for each
sample group.

Sample group	PVA wt%	FT cycles	Range of E (kPa)	Mean E (kPa)
1	4,3	2	6,4 - 6,6	6,5
2	4,8	2	8,9 - 9,0	8,9
3	4,8	1	2,3 - 2,5	2,4
4	5,2	1	5,7 - 5,8	5,8
5	5,7	1	8,0 - 8,2	8,0
Note. Young's modulus between a 19% - 29% strain				

Table 3.2: Range values of the Young's modulus (E) and the mean E of the PVA samples derived form the stress-strain curve

Using equation 3.1 the range values for the E* were calculated and are shown in Table 3.3. Comparing the E* from Table 3.3 with the E extracted from the stress-strain curve of Table 3.2, the desired wt% of the PVA can be selected. From the table it can be extracted that the brain phantom need to have an E between the range of 7,54 - 11,6 kPa, and the tumor phantom needs an E between the range of 3,48 - 6,38 kPa.

	μ (kPa)	v	E* (kPa)
Brain	3,3 ± 0,7	0,45	9,57 ± 2,03
GBM	1,7 ± 0,5	0,45	4,93 ± 1,45
Note. μ is the $|G^*|$ adopted from Pepin *et al.* [37]			

Table 3.3: Range values of the indicative Young's modulus

The E of the PVA samples in Table 3.2 can be examined and compared to the E* of the brain and tumor tissue in Table 3.3. Table 3.4 shows the calculated difference between the E resulting from the compression test and the E* extracted from the MRE data. The difference is described as ΔE*, as shown in the two right columns of Table 3.4. It can be seen that sample 2 only has a difference of +0,67 kPa between the E and E* of the brain tissue. Which means that the PVA sample is 7% softer than the actual brain tissue is. Sample 4 has a difference of -0,87 kPa between E and E* of the GBM. This indicates that the PVA sample is 17,6% stiffer than the actual GBM tissue is. These two samples have the smallest differences between the E and E*, and their corresponding mass fractions can be used for the production of the brain and tumor phantom, whereby a mass fraction of 4,8 wt% and two FT cycles will be the most suited for the brain phantom, and a mass fraction of 5,2 wt%, with one FT cycle, will be the most suited for the tumor phantom.

sample	PVA wt%	FT cycles	Mean E (kPa)	Δ E* brain	Δ E* GBM
1	4,3	2	6,5	+3,07	-1,57
2	4,8	2	8,9	**+0,67**	-3,97
3	4,8	1	2,4	+7,17	+2,53
4	5,2	1	5,8	+3,77	**-0,87**
5	5,7	1	8,0	+1,57	-3,07
Note. Δ E* = E* - E, whereby E* (brain) = 9,57 kPa and E* (GBM) = 4,93 kPa					

Table 3.4: Difference between E* found in literature and E determined with the compression test

3.2.3. Discussion and conclusion

In this section the determination of the stiffness of PVA samples was described. By comparing the E constructed from the compression test with the E* extracted from the literature the desired mass fraction can be determined. The first three requirements from subsection 3.1 were used as a guideline during this discussion.

At first, the stiffness of the brain phantom needs to be close to the real brain tissue as found in the literature. In Table 3.4 it can be seen that using 4,8 wt% PVA, and 2 FT cycles, has the closest mean E (8,9 kPa) compared to the E* (9,57 kPa). The difference between the mean E and E* is only +0,67 kPa, which means that the actual brain tissue is 0,67 kPa (7%) stiffer than the PVA sample. From this it can be concluded that by using this mass fraction a brain phantom can be created with a realistic stiffness compared with the actual brain.

Secondly, the stiffness of the tumor phantom needs to be close to the real GBM tissue as found in the literature. Table 3.4 shows that using 5,2 wt% PVA and 1 FT cycle has the closest mean E (5,8 kPa) compared to the E* (4,93 kPa). The difference between the E and E* is -0,87 kPa. This indicates that the actual GBM tissue is 0,87 kPa (17,6%) stiffer compared to the PVA sample. Despite the fact that the E and E* are not exactly the same value, the desired mass fraction and FT cycle can be used for the production of the tumor phantom. However, when looking at the percentage difference, it can be seen that the tumor phantom can be even better optimized in future research.

Lastly, materials with easily controllable mechanical properties are needed for the production of these PVA phantoms. By carrying out the compression test on the PVA samples, it was shown that the stiffness changed easily. However, due to the lack of information about the mechanical properties of PVA it is difficult to find the appropriate mass fraction for the associate stiffness. Nonetheless, through this experiment more clarity

has been found with regard to the stiffness of PVA. In Table 3.2 the range values of E are shown as extracted from the compression test. The range of these values is very small, and it can therefore be concluded that these values are very accurate. Using PVA for the production of a brain phantom is thus of great benefit to this master project because of the easily controllable stiffness.

From this section can be concluded that PVA is a advantageous material for the production of a brain phantom. The values of the stiffness are very accurate. Nevertheless, only 3 samples were made for each group, which is not that much. For future research it is recommended to make more samples per group, as well as more sample groups with different mass fractions. Still the data found during this experiment is very useful for future research and for the production process of the brain phantom.

3.3. Production process of the mould

The goal of this section is to describe the production process of the mould for casting the brain phantom. Firstly, the production method will be described. Then the mould will be shown in the results section. Lastly, a short discussion and conclusion will be provided in this section.

3.3.1. Method of production

The production method of F. Kor was used as a basis for the production of the head phantom [13]. F. Kor describes a method for creating a patient specific 3D model, segmented from a CT scan. The 3D model of the brain was used to create a negative image, in a solid structure, using Rhinoceros. The mould of the brain consist of 3 main parts; the bottom and two top parts, whereby the bottom part of the mould represents the superior part of the brain and the two top parts of the mould represent the inferior part of the brain. Figure 3.4 show the two top parts of the mould. In the right part two small holes are created to place a rod with a ball there, which is called the tumor insert. In Figure 3.5 the bottom part of the mould is shown, with the right top part with the tumor insert. The first hole at the anterior part of the mould was created by F. Kor. For the production of the first brain phantom the tumor insert was placed in the first hole. Moreover, for the second brain phantom the tumor insert was placed in the second hole, which was located more in the middle of the mould. The second hole was created in Rhinoceros. When the tumor insert gets removed, or dissolves, a hollow space is created in the brain phantom where the tumor phantom can be placed. In addition, the material of the tumor insert differs for the first and second phantoms created which will be further elaborated upon in the next subsection. The reason for the use of different materials and locations of the tumor insert is discussed in subsection 3.5.3.
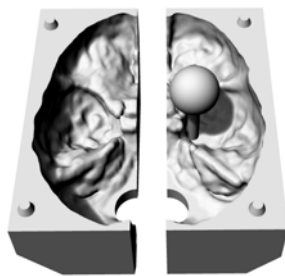
Figure 3.4: 3D image of the two top parts of the mould with the tumor insert in the second hole
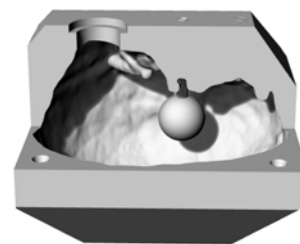
Figure 3.5: 3D image of the bottom mould, one top part and the tumor insert in the second hole

The mould for the tumor was the exact same mould that F. Kor created, which was the same way as the brain mould was created, but now a negative image of a round ball was created in Rhinoceros. This negative image was used to create the mould which consists of two parts; the top part and the bottom part, see Figure 3.6. At the top of the mould there is a small hole though which the PVA solution can be injected. Figure 3.7 illustrates the tumor mould when it is closed.

3D printing settings

As mentioned in section 2.6.4, 3D printing is a suitable method for the production of the moulds. The 3D images of the moulds, created in Rhinoceros, were exported to STL files. These STL files can be loaded into the 3D printing program Ultimaker Cura. Using this program the settings for the 3D printer can be made,
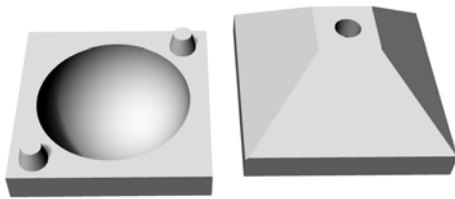
Figure 3.6: 3D image of the two tumor parts. Left: bottom part. Right: top part
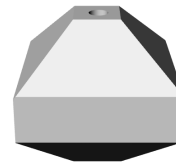
Figure 3.7: 3D image of the two tumor moulds closed

and the moulds can be printed. The moulds were printed using an Ultimaker 3E, 3 or 5 (Ultimaker BV, The Netherlands), which are located at the Faculty of Mechanical, Maritime and Material Engineering (3mE). These printers use FDM technology. The build material is PLA (Ultimaker BV, The Netherlands) and the support material is PVA (Ultimaker BV, The Netherlands) [61]. The moulds and tumor inserts are build of PLA build material for the production of the first brain phantom. However, for the production of the second brain phantom the tumor insert material was changed to the support material PVA for the use case. Here the tumor insert is a water soluble material where it can dissolve in water once the brain phantom is made. The exact setting for each print can be found in Appendix C and the exact sizes for each structure can be found in Appendix D.

Post-processing

The 3D printed moulds are not watertight and therefore post-processing is needed. By coating the moulds with XTC-3D$^{\text{TM}}$ Coating (Smooth-On, USA) the mould will be watertight [62]. It is important that when the mould is to be used multiple times, the mould needs to be re-coated every time prior to the use. Otherwise the mould will not be watertight and the PVA solution will leak through the mould, which happened during the second production of the brain phantom for the use case. A leak between moulds must also be prevented. This can be done by applying a large amount of petroleum jelly (Vaseline, The Netherlands) between the moulds. Thereafter, the moulds need to be firmly taped together using duct tape (Tesa, Germany).

3.3.2. Results

The printed mould of the brain is shown in Figures 3.8 and 3.9. Figure 3.8 shows the two top parts of the moulds. The grey mould represents the left inferior part of the brain and the white mould represents the right inferior part of the brain. In the white mould the tumor insert of PVA is placed. As can be seen here there are two holes for the tumor insert. The PVA tumor insert is placed in the second hole in the figure. In Figure 3.9 the bottom part of the mould is shown which represents the superior part of the brain. Figure 3.10 shows the two parts of the tumor mould. Whereby the left mould is the bottom part of the tumor mould and the right mould the top part.

Figure 3.8: The two top parts of the brain mould with the tumor insert

Figure 3.9: The bottom part of the brain mould

Figure 3.10: The two parts of the tumor mould

3.3.3. Discussion and conclusion

In this subsection the production of the mould will be discussed. A patient-specific mould for a brain phantom was 3D printed. The production method and 3D model design was partly in accordance with the thesis of F. Kor. However, some adjustments were made in the 3D model. Using a 3D printing technique, the production process of the mould was fast, easy and low cost. Nonetheless, printing the PVA tumor insert came with a complication. Since the build material and the support material were both of the same material, this made it more difficult to remove the support material without removing parts of the tumor insert itself. Furthermore, the brain mould was leaking, even though the post-processing was carried out. One of the reasons is that each time the mould is used, it needs to be coated again. This is another reason why the mould design is not perfect and needs to be improved. This will be further discussed in section 5.2.

3.4. Production process of the skull

In this section the production process of the skull phantom will be described. At first, the production method will be explained. Then, in the results section, the skull will be shown. Finally, a discussion and conclusion will be provided.

3.4.1. Method of production

The production method of F. Kor was also used as the basis for the production of the skull. Figure 3.11 illustrates a 3D image of the skull. Using Rhinoceros the 3D model of the skull, created by F. Kor, was edited, whereby the skull was sliced into two in the middle as the top needs to be removable from the whole skull to place the brain phantom in. The skull consists of the following parts; the skull top, the skull base and the jaw. To attach the skull top and skull base, cone pins were fixated in the 3D model of the skull base, and cone holes were made in the skull top. Figure 3.12 shows the 3D model of the skull top and Figure 3.13 shows the 3D model of the skull base.

Figure 3.11: 3D image of the whole skull   **Figure 3.12:** 3D image of the skull top   **Figure 3.13:** 3D image of the skull base
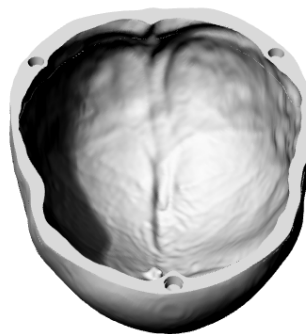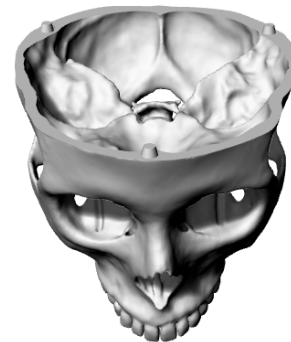
3D printing settings

For the production of the skull, the same 3D printing method was used as those for the production of the moulds. Using PLA $CaCO_3$, as build material for the skull, should have been the most suitable material for the visibility in a CT scan. However, due to an error in the 3D printer, and therefore the shortage of time, the skull was printed using normal white PLA. In addition, to mimic a real skull and to make the skull model firm, the infill and layer thickness needs to be more compact compared to the mould. The exact setting for each print can be found in Appendix C and the sizes can be found in Appendix D.

Post-processing

Due to the complex structure of the skull, a lot of support material is needed during the printing process. Therefore, the printed skull phantom needs to soak in a bucket with water for 2 consecutive days after printing, which is needed to remove all the PVA support material. When the PVA solution is dissolved the skull

phantom does not need post-processing and the skull phantom is ready for use. However, after placing the brain phantom in the skull, the skull top and the skull base need to be fixated. The fixation of the skull can be done using universal kit adhesive (Bison, Canada). The kit keeps the two parts together, but by using a flat thin object, such as a knife, the skull top and skull base can still be detached. Normally the adhesive should be strong enough to bind the two parts together, but, because of the wetness of the brain phantom inside the skull the kit is somewhat less adhesive, which is an advantage because the skull can be reused.

3.4.2. Results
The frontal view of the printed skull phantom is shown in Figure 3.14 and the lateral view is shown in Figure 3.15. As shown the skull top and skull base fit perfectly onto each other through the cones. However, this is not fixated enough to stay in place during movement. Figure 3.16 demonstrates the three parts of the skull phantom; the jaw on the left, the skull base in the middle and the skull top on the right.

Figure 3.14: Anterior view of the skull phantom

Figure 3.15: Lateral view of the skull phantom

Figure 3.16: The 3 parts of the skull phantom. Left: the jaw. Middle: skull base. Right: skull top

3.4.3. Discussion and conclusion
In this section the production of the skull phantom has been described. The skull phantom consist of 3 parts; the jaw, the skull top and the skull base. The skull top can be removed from the skull base, allowing the brain phantom to be placed in the skull. However, when the skull phantom is used during which a hole will be drilled, it is not fully reusable and a new top needs to be printed. However, during the design phase there was no focus on one particular type of surgery and therefore there was no permanent drilling place.

Though the 3D printing technique a patient-specific skull phantom can be manufactured. Nonetheless, because the skull has a complex structure, it took a long time printing and had a bigger risk of failure. This should be taken into account during the production of the skull phantom. Nevertheless, 3D printing is the most suitable and accurate method to create a skull phantom.

The skull phantom needs to have sufficient contrast for it to be seen in a CT scan. Preferably the skull phantom can mimic the bony parts of the skull in the CT. According to the literature mentioned in subsection 2.6.5, PLA CaCO$_3$ would be a suitable material to create contrast. However, through a lack of time and the error in the 3D printer, the skull phantom was printed using normal PLA. The contrast of the skull phantom will be shown and discussed in section 4.3, where a CT scan was carried out.

3.5. Production of the brain phantom
The goal of this section is to describe the production process of the brain phantom. Firstly, the method of production will be described. Secondly, the brain phantom will be shown in the results section. Lastly, in the discussion and conclusion section the production process will be discussed.

3.5.1. Method of production
In section 3.2.1, the stiffness of PVA samples were compared to the stiffness of the brain. As a result of the mechanical tests, the desired mass fractions were found to mimic brain and GBM tissue. The corresponding

mass fractions were discussed in subsection 3.2.3, of which the brain phantom can be produced by using 4,8 wt% PVA, with 2 FT cycles, and the tumor tissue can be produced with 5,2 wt% PVA, with 1 FT cycle. Table 3.5 shows the proportions and quantities needed for the production of the brain phantom. In Table 3.6 the proportions and quantities needed for the production of the tumor phantom are shown. The weight of the required substances is expressed in grams. As the volume of the tumor is 17 mL, only a small amount of PVA solution is needed. However, when a small amount of PVA solution is made, the solution evaporates very quickly. Thereby, a larger amount of the solution is made from which two tumors phantoms can be made. See Appendix B for an elaboration of the production method of the PVA. After the phantom had thawed to room temperature the tumor insert was removed from the phantom, and the tumor phantom was subsequently inserted into the phantom.

	Water	Coolant	PVA
Weight (g)	1200	300	75,6
Mass Fraction (wt%)	76,2	19,0	4,8

Table 3.5: Proportions and quantities for the brain phantom of approximately 1,6 L

	Water	Coolant	PVA
Weight (g)	36	9	2,46
Mass Fraction (wt%)	75,8	19	5,2
Note. This amount is to produce 2 tumor phantoms			

Table 3.6: Proportions and quantities for the tumor phantom of approximately 0,5 L

3.5.2. Results
The brain and tumor phantom were created using the proportions from Table 3.5 and 3.6, with the production method described in Appendix B. In Figure 3.17 the brain phantom is shown when it is still partly in the mould. Unfortunately, a part of the PVA solution leaked through and therefore the shape of the brain phantom is anatomically incorrect. The picture was taken when the brain phantom was still frozen. Figure 3.18 shows the lateral view of the brain phantom. In Figure 3.19 the tumor phantom is shown. The tumor was still frozen when this picture was taken. When the tumor insert was removed from the brain phantom, the phantom tore open a bit. Therefore the tumor phantom did not stay in place in the brain phantom. Figure 3.20 shows the brain phantom placed in the skull. See Appendix E for more figures of the phantom.

Figure 3.17: Brain phantom in the mould

Figure 3.18: Lateral view of the brain phantom

3.5.3. Discussion and conclusion
In this subsection the production of the brain and tumor phantom will be discussed. Some of the requirements described in subsection 3.1 will be used as a guideline to discuss the production process.

At first, the stiffness of the brain and tumor phantom need to be close to the actual tissue of the brain and tumor. For the production of the brain and tumor phantom the mass fractions from section 3.2 were used. In that section it was discussed that the stiffness was close to the actual brain and tumor tissue.

Figure 3.19: Tumor phantom

Figure 3.20: Brain phantom in the skull

Secondly, the phantom needs to be easy and inexpensive to manufacture. Due to the 3D printing technique a patient-specific mould was printed for the brain phantom. This was an inexpensive and fast technique. However, during the production of the brain phantom the mould was leaking. This caused the production process to take longer than expected, with the consequence that the brain phantom did not have the right anatomical shape. Further, PVA is an expensive material (€0,416 per gram) so when multiple brain phantoms are created, the production costs will not be low [63]. Thus, the manufacturing technique may be easy but for future research the moulds need some improvements in order to stop the leaking.

Lastly, there should not be any displacement of the tumor phantom in the brain phantom, during the production process. Unfortunately, the brain phantom physically tore when the tumor insert was removed from the brain phantom. Through this the tumor did not stay in place. The PVA brain phantom is very soft and tears easily. Therefore it is better when the tumor phantom is less close to the surface of the brain phantom. Therefore, the location of the tumor insert needs to be changed. Another method to prevent the brain phantom from tearing is by changing the material of the tumor insert. This will be discussed in section 4 where a new phantom is made for an use case.

4

Specific use case for the head phantom

The goal of this chapter is produce a brain and tumor phantom for the use case of a project from the TU Delft and Utrecht university. During the use case the HoMS administration device, and a stereotactic frame (created by M. de Vries) will be evaluated, and a CT and MRI scan will be carried out. Firstly, the production of the phantom that was needed for the use case in particular is described. Secondly, general information about this experiment is provided. Then the experiment, using the CT scan ,is described and the results are shown and discussed. Thereafter the experiment using the MRI scan is elaborated upon, and the MRI images are shown and discussed. Lastly, a mechanical test was carried out on new PVA samples containing $BaSO_4$.

4.1. Production of the brain phantom for the use case

The goal of this section is to describe the production process of the brain phantom for this specific use case. Firstly, the production method will be described. Then the brain phantom will be shown in the results section. Lastly, in the discussion and conclusion section, the production process will be discussed.

4.1.1. Method of production

For this specific use case a head phantom was needed with visible CT and MRI contrast. This allows the knowledge obtained during this thesis project to be immediately put into practice. Through previous research done during this master project a brain phantom, with comparable stiffness to the actual brain and GBMs, can be produced. However, some adjustments were needed to optimize the brain phantom for this specific use case. Firstly, the location of the tumor insert was changed and placed more to the middle of the mould. Because of this the tumor is also located more in the middle of the brain. The second adjustment was that the tumor insert was printed with PVA support material, in order to let it dissolve after the brain phantom was made. Thirdly, $BaSO_4$ was added to the PVA solution for improving the contrast of the brain and tumor phantom in the CT scan. Lastly, the mould had to stop leaking. This was done by adding more petroleum jelly between the parts of the mould and taping these more firmly together.

The production method of the PVA solution for the brain phantom was almost the same as done previously, except now $BaSO_4$ was added. According to the literature in section 2.6.5, $BaSO_4$ can create a realistic contrast for CT scans. Therefore, $BaSO_4$ was added as 1 wt% of the total weight of the brain mixture, and 2 wt% of the total weight of the tumor mixture. Furthermore, the mass fraction of the PVA, and the FT cycles, in the brain and tumor phantom were the same as described in subsection 3.5. Table 4.1 shows the proportions and quantities needed for the production of the brain phantom with $BaSO_4$ added, whereby the weight of required substances is expressed in grams. Table 4.2 shows the proportions and quantities needed for the production of the tumor. Again two tumors were made because using too small amounts of the PVA solution causes it to evaporate. The production method is explained, step-by-step, in Appendix B.

4.1.2. Results

In Figure 4.1 the brain phantom is shown in the mould. The brain phantom was still frozen when the picture was taken. As can be seen in the picture the mould was still leaking. Therefore a clay filling was made to fill up the bottom of the brain in the skull, as shown in Figure 4.3. In Figure 4.2 the superior part of the

	Water	Coolant	PVA	BaSO$_4$
Weight (g)	1200	300	75,8	15,9
Mass Fraction (wt%)	75,4	18,8	4,8	1,0

Table 4.1: Proportions and quantities for the brain phantom with BaSO$_4$ of approximately 1,6 L

	Water	Coolant	PVA	BaSO$_4$
Weight (g)	40	10	2,8	1,0
Mass Fraction (wt%)	74,2	18,6	5,2	2,0
Note. This amount is to produce 2 tumor phantoms				

Table 4.2: Proportions and quantities for the tumor phantom of approximately 0,5 L

brain phantom is shown. The white substance is the undissolved BaSO$_4$ that lowered down after pouring the solution in the mould. The tumor phantom made with BaSO$_4$ immediately fell apart after thawing the tumor phantom to room temperature. Therefore, the tumor produced without the BaSO$_4$ addition, as produced in section 3.5 was used for this use case. This will be discussed further in subsection 4.1.3. Since the tumor without the BaSO$_4$ addition will be used for the MRI and CT scans, small marker points were needed to be inserted in the tumor. Therefore, small aluminum balls were pushed inside the tumor with a needle when the tumor had thawed.
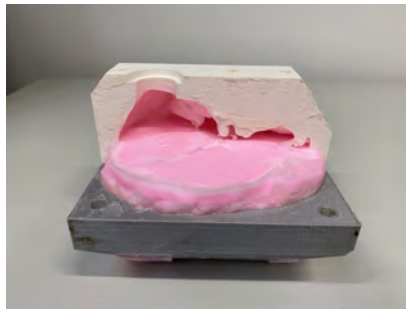

Figure 4.1: Brain phantom in the mould

Figure 4.2: Superior of the brain phantom

Figure 4.3: Clay filling in the skull

4.1.3. Discussion and conclusion

In this section the production of the brain and tumor phantom for the use case will be discussed. The requirements described in subsection 3.1 were used as a guideline during the design phase.

Firstly, the stiffness of the brain and tumor phantom needs to be comparable to real brain and GBM tissue. Through the mechanical testing, and by comparing it with the literature, the mass fractions, as close to the real brain and GBM tissues as possible, were selected and used for the production of this brain phantom. Through this a brain phantom was created with a stiffness close to the actual human brain.

Secondly, the production method needs to be inexpensive and easy to manufacture. A short discussion was already provided in subsection 3.5.3. However, after improving the mould it was still leaking. This shows that the design of the mould needs to be improved. In addition, the mould must be re-coated every time a new brain phantom is made. Though the leaking mould the brain phantom did not have the right anatomical shape. This makes the production process of the brain phantom less easy than expected.

Thirdly, it is required to have CT contrast for the brain and tumor phantom. Literature has shown that a PVA phantom with BaSO$_4$ has a comparable contrast for CT [55]. In subsection 4.3 the contrast of the BaSO$_4$ will be shown and discussed. Nonetheless, during the production of the brain and tumor phantom some flaws regarding the use of BaSO$_4$ have been found. Firstly, the BaSO$_4$ did not dissolve in the PVA solution. As a consequence the BaSO$_4$ emerged in the bottom of the mould and was not evenly divided. Secondly, when 2 wt% BaSO$_4$ was used in the tumor phantom, the PVA stayed too soft after 1 FT. This could explain why the PVA could not make the cross-links and therefore why the tumor phantom stayed too soft. Therefore, the tumor

with 5,2 wt%, 1 FT, and without the addition of $BaSO_4$, as per section 3.5 was used for this experiment.

Lastly, there should not be any displacement of the tumor phantom during the production process. Through the adjustments of the location and the material of the tumor insert, the hole for the tumor did not tear. Therefore, the tumor was not displaced after being placed into the brain phantom.

4.2. Experiment at Utrecht University

For a parallel project at the TU Delft and the Faculty of Veterinary Medicine at Utrecht University a head phantom was required. This phantom was needed to test and evaluate the HoMS administration device and a stereotactic frame created by M. de Vries [49]. An experimental set-up was made using a specific head phantom, the stereotactic frame and the HoMS administration device. Together with researchers N. Klaassen, C. Morsink and M. de Vries, because of this use case important aspects for this master thesis could be examined, including whether the brain phantom was CT and MRI compatible, and where the movement of the brain and tumor during the insertion of the needle and the whole head phantom could be evaluated. In addition, other aspects were examined with regard to the evaluation of the stereotactic frame and HoMS administration device, such as potential disturbances on the images, workflow optimization and the ease of use. A total of 9 CT scans and 2 MRI scans were carried out during this experiment, whereby 1 MRI scan was made before the experiment, and the CT scans and 1 MRI scan were made after the experiment.

As mentioned in section 2.5, M. de Vries developed an HoMS administration device for the brachytherapy brain tumors and this device was used during the experiment. The HoMS administration device has been used for the treatment of brain tumors in dogs at the Small Animal Clinic Utrecht, because of the many similarities between the brain structure and tumor characteristics of humans and dogs. This resulted in some good outcomes and has recently led to the experimental treatment of humans with head and neck tumors at the University Medical Center Utrecht [48]. The stereotactic frame, created by M. de Vries, was originally developed for the treatment of dogs. However, during the experiment a head phantom was required to evaluate the frame. This created a 3 dimensional reference system for the planning and navigation of the needle during the experiment. In Figure 4.4 and 4.5 the stereotactic frame, the head phantom and the cannula of the administration device are shown.
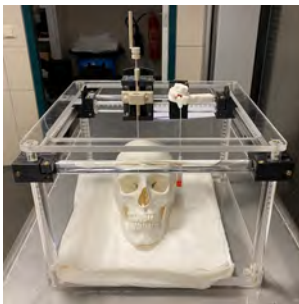
Figure 4.4: Anterior view of the head phantom, stereotactic frame and the cannula
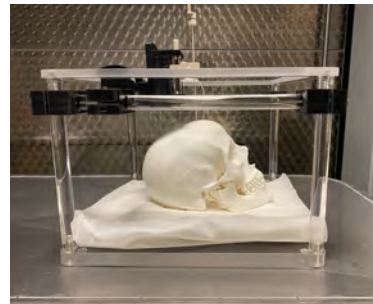
Figure 4.5: Lateral view of the head phantom, stereotactic frame and the cannula

4.2.1. Materials

The various types of instruments, specimen and equipment used for the experiment are described in the subsections below.

Instruments

The brain phantom consists of 4,8 wt% PVA and 1 wt% $BaSO_4$ and was subjected to 2 FT cycles. Within the brain phantom a tumor phantom is placed. This tumor phantom is made of 5,2 wt% PVA and was subjected to 1 FT cycle. The skull of the head phantom is made of PLA. The transparent part of the Socratic frame, as shown in Figure 4.6 (by M. de Vries) is made of polymethylmethacrylate (PMMA) which is an MRI and CT compatible material. The parts that need to be sterilized are constructed of polyether ether ketone (PEEK). Furthermore, the fixation and movement parts of the frame are 3D printed with PLA and brass bolts and nuts

have been used. The stereotactic frame has the following dimensions: 395 × 410 × 320 mm (L × W × H) In Figure 4.7 the HoMS administration device is shown. The cannula is made of bioceramix alumia oxide (99,8%), with a PEEK handle and a silicon O-ring. The dimensions of the cannula are as follows: the outer diameter is 1,60 mm, the inner diameter is 0,80 mm and the length is 153,5 mm. The pre-bend stylet (Cook Medical, USA) consists of super elastic nitinol with the following dimensions: the outer diameter is 0,260 mm, the inner diameter is 0,514 mm and has a radius of 15 mm over $0,5\,\pi$.

Figure 4.6: Stereotactic frame with the cannula in it

Figure 4.7: Cannula needle with pre-bend stylet

Specimen
In this experiment, 145 mg holmium loaded poly(L-lactic acid) microspheres (HoPLLAMS), dissolved in Pluronic F68, has been used as the injection suspension. Only 87 mg of the HoPLLAMS was needed for inside the tumor. During the experiment, at the CT scan, 12 depots of the suspension were done.

Equipment
The Somatom Definition Edge CT scan (Siemens, Germany) and the Ingenia 1.5T MRI scan (Philips, The Nether- lands) at the Faculty of Veterinary Medicine at Utrecht University were used during this experiment. First the MRI was used to make a scan of the head phantom with the frame and cannula. Then the CT scanner was used to make multiple scans during the insertion of the administration device and the injection of the HoPLLAMS suspension. Lastly, a MRI scan was made again after the injection of the HoPLLAMS. Additionally, a 18V Lithium Ion drilling machine (Black+Decker, USA) was used to drill a small hole in the skull in order to iinsert the cannula into the brain phantom. In order to fixate the skull to the stereotactic frame, masking tape (Tesa, Germany) was used. The MRI and CT images were made using the online program Horos.

4.3. CT scan
The goal of this section is to describe the experiment that was carried out with the CT. At first, the experimental set-up and protocol will be explained. In the results section the CT images will be shown. Lastly, a discussion and conclusion will be provided with the requirements as a guideline.

4.3.1. Experimental protocol
Firstly, it was checked whether the instruments, specimens and equipment were present. Secondly, the experimental set-up was build, as shown in Figure 4.8 and 4.9. In order to do so the head phantom had to be placed in the stereotactic frame and fixated with tape. A ceramic needle was placed in the frame, approximately at the height of the tumor phantom, as a reference point.

The stereotactic frame was placed in the CT and the first CT scan (CT1), with 400 mAs, was made to localize the exact location of the tumor. Using CT1 the X,Y,Z coordinates were calculated and adjusted in order to place the needle exactly above the tumor. The second CT scan (CT2), with 400 mAs, was made to verify whether the location of the needle was correct. Then a burr-hole was drilled into the skull with a diameter of 4 mm. The cannula with the stylet were placed in the stereotactic frame and were partly inserted into the brain phantom. After this the third CT scan (CT3), with 400 mAs, was made to calculate the desired displacement in the z-direction in order to let the tip of the cannula touch the edge of the tumor. Through the calculations the cannula was moved down in the z-direction. The fourth CT scan (CT4), one with 400 mAs, and one free mAs, was made of the cannula on the edge of the tumor. Then the cannula was moved 1.5 cm down in the
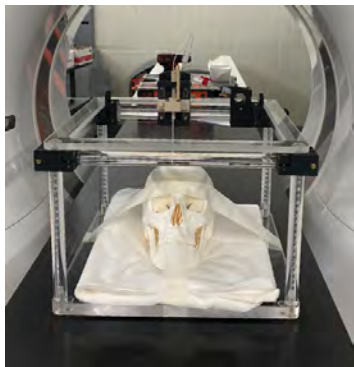
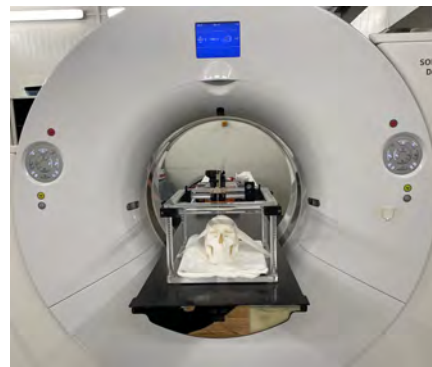**Figure 4.8:** A closeup of the experimental set-up in the CT scan

Figure 4.9: The experimental set-up in the CT scan

z-direction in order to place the cannula at $\frac{2}{3}$ of the tumor. The fifth CT scan (CT5), with 400 mAs, was made to check whether the location was correct and to compare this with CT4 to check whether the tumor was displaced during the penetration of the cannula. Then the stylet needle was brought in position in order to inject the HoPLLAMS suspension. At the first round of injections, 6 injections were placed in the tumor. Through rotating the stylet 3 injection places were used and on each place two injections were done; one at the maximum position and one at the minimum position of the stylet. After the first round of injections at the lower part of the tumor the sixth CT scan (CT6), with 400 mAs, was made to verify where the HoPLLAMS suspension in the tumor was located. Thereafter, the cannula was moved 0.5 cm up in order to place the cannula at $\frac{1}{3}$ of the tumor and the seventh CT scan (CT7), with 400 mAs was made. After CT7 the second round of injections was done in the same way as before. As a result, the tumor had been injected 12 times, at two different heights. Figure 4.10 illustrates the injection places of the tumor. The Cannula and stylet needle were then removed from the brain phantom. The eight CT scan (CT8), with 400 mAs, and the ninth CT scan (CT9), with free mAs, were carried out to localize the suspension after the two injection rounds.
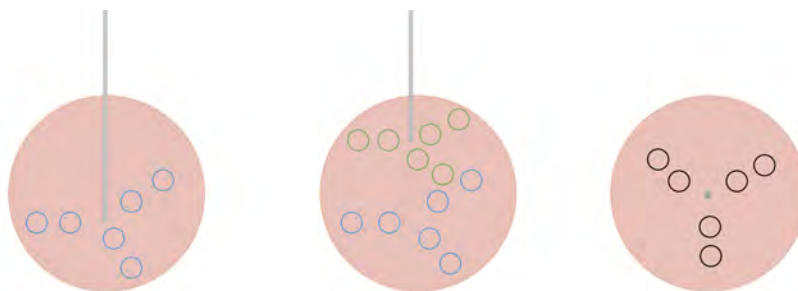
Figure 4.10: The injection rounds. Left: The first injection round (blue circles) at $\frac{2}{3}$ of the tumor. Middle: The second injection round (green circles) at $\frac{1}{3}$ of the tumor. Right: superior view of the places of the injections

4.3.2. Results

As described in the previous subsection, 9 CT scans were carried out during the experiment. The two most relevant CT scans were CT4 and CT5. These CT scans were made to examine whether there was any movement of the tumor when the cannula was inserted into the tumor phantom. Figure 4.11 shows CT4 image in a coronal plane with a frontal view of the head phantom. The tip of the cannula is at the edge of the tumor. The aluminum marker point is shown on the left side of the tumor. Between the tumor and the brain a black hole can be seen which is probably an air bubble. The clay that was used to fill up the bottom of the brain phantom can be clearly seen at the CT, but it did not influence the CT scan. In Figure 4.12 the CT5 is shown in a coronal plane with an anterior view of the head phantom, where the cannula penetrated the tumor phantom. As can seen in the CT image, the tumor phantom did not move, or fall apart, after the penetration. The difference in contrast between the tumor and brain phantom can hardly be seen in the CT images. Also the skull is almost invisible.

Figure 4.11: CT4 in coronal plane, anterior view. The cannula at the edge of the tumor

Figure 4.12: CT5 in coronal plane, anterior view. The cannula at $\frac{2}{3}$ of the tumor

The other two CT scans that are interesting for future research were CT6 and CT8, whereby CT6 is the scan after the first injections round as is shown in Figure 4.13. In Figure 4.14 CT8 is shown after the second injections round. Both CT im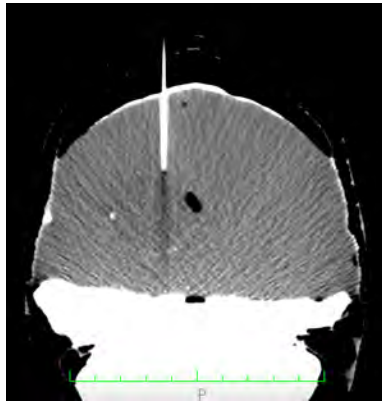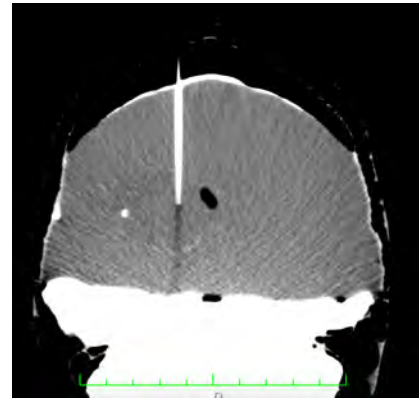ages are in a coronal plane with an anterior view of the head phantom. As can be seen in the images the HoPLLAMS suspension sunk to the bottom of the tumor phantom. See Appendix F for more CT images.
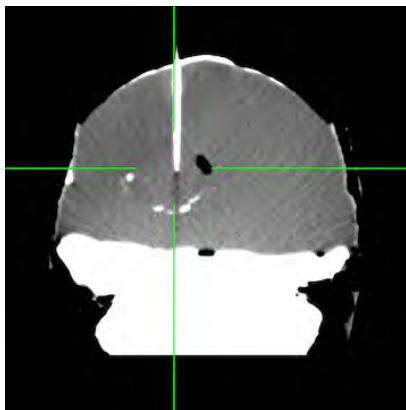
Figure 4.13: CT6 in coronal plane, anterior view. After the first injection round

Figure 4.14: CT8 in coronal plane, anterior view. After the second injection round

4.3.3. Discussion and conclusion

In this subsection the experiment with the CT scan will be discussed. Some of the requirements of section 3.1 were used to discuss this experiment.

Firstly, it is required that the brain and tumor phantom have CT contrast. In the CT images a contrast is shown in the brain and tumor phantom. However, there is no difference in contrast between the brain and the tumor phantom. The tumor shows the same contrast as the brain does, and thus it cannot be concluded from the CT images whether there is a difference in mechanical properties between the tumor and brain. At the superior part of the brain a bright layer is shown. This is the $BaSO_4$, that was used as a contrast additive. As the $BaSO_4$ did not dissolve during the production of the brain phantom it is only showing this at the superior part of the brain phantom. At the inferior part of the phantom the clay is shown. For future research the production of the moulds needs to be improved in order to make an anatomically correct phantom without a clay filling. The skull is not visible in the CT images however, which contradicts some literature. According to literature a PLA skull phantom should be slightly visible in a CT scan [13][15]. However, a PLA $CaCO_3$ skull phantom should be more visible, and should therefore be used for future research when a skull phantom is produced.

Secondly, the tumor phantom has to stay in place of the brain phantom during the production process. In the CT scan it is shown that before the cannula was inserted the tumor was in place correctly and the brain phantom was closely surrounded by the tumor. Additionally, the tumor phantom did not displace when the cannula was inserted into the tumor phantom. It can therefore be concluded that there is no displacement of the tumor during the production process, and that it fits firmly in the brain. This can be of great interest for future research when testing and evaluating new medical devices.

4.4. MRI scan

The goal of this section is to describe the experiment that was carried out with the MRI. Firstly, the experimental set-up and protocol will be described. Then the results of the MRI scan will be shown in the results section. Lastly, a discussion and conclusion section will be provided.

4.4.1. Experimental protocol

As mentioned in section 4.2, 2 MRI scans were carried out. The first MRI scan (MRI1) was made before the experiment took place with the CT scans mentioned above. The second MRI scan (MRI2) was made after the experiment with the CT scans. First it was checked whether all the instruments and equipment were present. Secondly the first impression of the stereotactic frame and the head phantom were evaluated. After that the experimental set-up was build as shown in Figure 4.4 and 4.5. The head phantom was placed in the stereotactic frame and the cannula was fixated in the frame. Then the stereotactic frame was placed in the MRI, with the anterior side of the head facing the MRI scanner, see Figure 4.15. The two coils were fixated to the head phantom with tape.

Figure 4.15: MRI scan with the stereotactic frame, head phantom and cannula

Then MRI1 was made with a slice thickness of 5 mm T_1, T_2 and T^* weighted. After the MRI1 the experiment described in section 4.3 was carried out. After the CT experiment the stereotactic frame and head phantom were placed in the MRI scanner again. MRI2 was done to examine whether the substance was still in the tumor or whether it had been displaced.

4.4.2. Results

As described in the previous subsection two MRI scans were carried out. MRI1 T_2-weighted image is shown in Figure 4.16, in a coronal plane with an anterior view. The two aluminum marker points are shown in the tumor and the tumor is clearly visible. The brain and tumor phantom show clear MRI contrast. At the superior part of the brain phantom a darker part is showing, which is the undissolved $BaSO_4$. However the skull phantom gives little signal in the MRI scan and is therefore poorly visible. In Figures 4.17 and 4.18 MRI2 T_2-weighted images are shown in a coronal plane with an anterior view. This MRI was carried out after the injection of the HoPLLAMS substance. The MRI image shows that the substance had settled down. The tumor had become detached from the brain phantom, which may be caused by the sagging substance. See Appendix F for more MRI images.
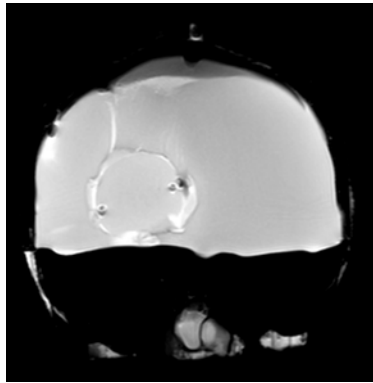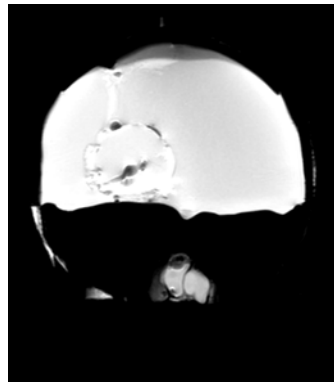
Figure 4.16: MRI1, T_2-weighted

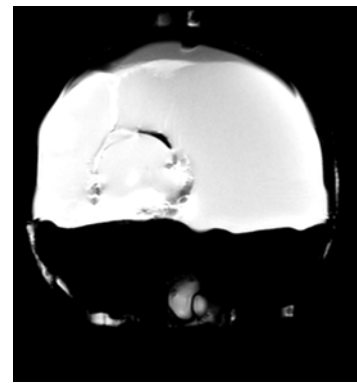**Figure 4.17:** MRI2, T_2-weighted

Figure 4.18: MRI2, T_2-weighted

4.4.3. Discussion and conclusion

In this subsection a discussion and conclusion will be provided about the MRI of the head phantom. Some of the requirements of section 3.1 were used to discuss the results of the MRI.

Firstly, it is required that the head phantom has MRI contrast. The brain has a good visibility in the MRI scan. However, the undissolved $BaSO_4$ is darker compared to the other part of the brain. Therefore, $BaSO_4$ is not needed for the production of a brain phantom to create sufficient MRI contrast. The tumor phantom is clearly distinguishable from the brain, and the marker points were not needed to localize the tumor in the MRI. However, a difference in contrast between the brain and tumor is not visible. This can be caused by two different things. At first, the difference in stiffness between the tumor and brain is too small, so that no contrast difference is showing. The other reason may be that some of the $BaSO_4$ did partly dissolve in the brain phantom. This results in a darker brain image then would be the case normally. If that is the case, then the tumor phantom is less stiff compared to the brain phantom. This correlates with the findings in section 4.1, where the compression test indicated that the tumor should be less stiff compared to the brain phantom. The skull phantom was poorly visible in the MRI. For future research the skull could be coated with glue, or a greasy substance, or printed with a photopolymer resin in order to create more contrast [64].

Using the CT scan it was proven that the tumor stayed in place during the production process. However, looking at the MRI scan, it can be seen that, after an injection with the HoPLLAMS substance, the tumor phantom got detached from the brain phantom. Additionally, the HoPLLAMS substance sank in the tumor phantom. This should be investigated further in future research, in order to examine whether the tumor and brain phantom behave in the same way as actual tissue does. This will be elaborated upon in section 5.2 where the recommendations will be discussed.

4.5. Mechanical testing of PVA samples with $BaSO_4$

The goal of this section is to determine the stiffness of the PVA samples with $BaSO_4$ that were used to produce the brain and tumor phantom in the use case. A mechanical test was carried out after the use case. Firstly, the method of production will be described. Secondly, the results will be shown and the Young's modulus will be calculated. Lastly, a discussion and conclusion section will be provided.

4.5.1. Method of production

The PVA solution, that was left over from the production of the brain and tumor phantom with $BaSO_4$, was poured into the same square moulds as used in section 3.2.1. The squares were subjected to the same number of FT cycles as the brain or the tumor were (depending on the one the solution was a left over from). New PVA samples, with $BaSO_4$, were made to perform a mechanical test. The same compression test was done as on the previous PVA samples, which is explained in subsection 3.2.1. Using the compression test a stress-strain curve can be identified and the Young's modulus can subsequently be calculated. Because of this it can be examined whether there is a change in stiffness when $BaSO_4$ is added to the PVA solution.

4.5.2. Results

As a result of the compression test, that was carried out on the PVA samples with BaSO$_4$, two new stress-strain curves were added to Figure 4.19. The two striped lines represent the PVA samples with BaSO$_4$. In Figure 4.20, four stress-strain curves are illustrated. There the two red lines (sample 2 and 6) represent both the 4,8 wt% 2 FT PVA samples used for the brain phantom, and the black lines (sample 4 and 7) are the 5,2 wt%, 1 FT, PVA samples used for the tumor phantom. From the stress-strain curve it can be inferred that using BaSO$_4$ leads to a reduction in the stress-strain curve. See Appendix A for more stress-strain curves of the PVA samples.
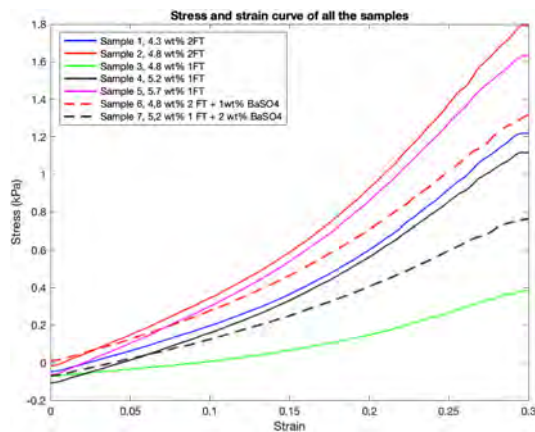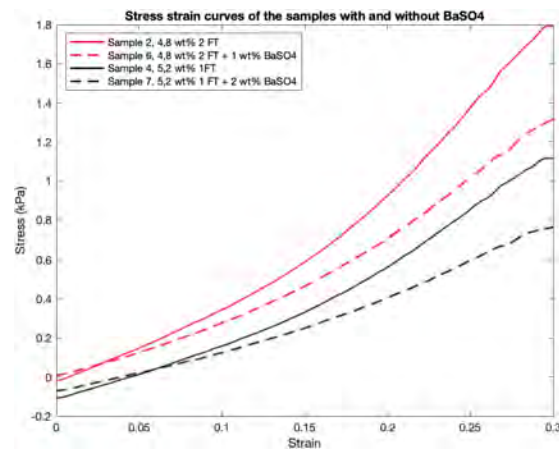

Figure 4.19: Stress-strain curve of all the samples

Figure 4.20: Stress-strain curve of the samples with/without BaSO$_4$

The Young's modulus of the two samples are derived from the slope of the stress-strain curve. Table 4.3 shows the E of the two samples with BaSO$_4$ (sample 6 and 7), and the E without BaSO$_4$ (sample 2 and 4). Sample 2 and 6 have the same PVA mass fraction and this should be the mass fraction to mimic the brain tissue. Sample 4 and 7 have the same PVA mass fraction, and this should be the mass fraction to mimic the tumor tissue. However, in the table is shown that the E changes when BaSO$_4$ is added. It should also be noted that sample 6 represents the sample of the brain phantom and sample 4 represents the sample of the tumor phantom used during the case study.

Sample	PVA (wt%)	FT cycle	BaSO$_4$ wt%	Range of E (kPa)	Mean E (kPa)
2 (red line)	4,8	2	0	8,9 - 9,0	8,9
6 (red striped line)	4,8	2	1	6,0 - 6,2	6,1
4 (black line)	5,2	1	0	5,7 - 5,8	5,8
7 (black striped line)	5,2	1	2	3,6 - 3,9	3,7
Note. For this use case: Sample 6: Brain phantom. Sample 4: Tumor phantom					

Table 4.3: Young's modulus of the two samples with BaSO$_4$ and two samples without BaSO$_4$ from Figure 4.20

As can be seen in the table the Young's modulus changes when BaSO$_4$ is added to the PVA samples. The mean Young's modulus of the brain phantom, with BaSO$_4$ in the use case (E = 6,1 kPa), is 2,8 kPa lower compared to the brain phantom without BaSO$_4$. When comparing the E to the indicative Young's Modulus (E* = 9,57 kPA) of the real brain tissue, this results in that the brain phantom with BaSO$_4$ is 3,47 kPa lower than expected. In addition, the Young's modulus of the tumor phantom changed as well when the BaSO$_4$ was added to the PVA sample. The Young's modulus tumor phantom with BaSO$_4$ (E = 3,7 kPa) is 2,1 kPa lower than the tumor phantom without BaSO$_4$ (E = 5,8 kPa) is. However, it should be noted that a tumor phantom without BaSO$_4$ was used for this use case.

4.5.3. Discussion and conclusion

In this subsection the mechanical test on the PVA samples with BaSO$_4$ will be discussed. This is done by using some of the requirements from section 3.1 as a guideline.

At first, the stiffness of the brain phantom need to be close to the actual brain tissue. At first it was aimed for to recreate the first brain phantom with a mean E of 8,9 kPa. However, by adding BaSO$_4$ the stiffness of

the PVA brain phantom changed. Therefore, the brain phantom in this use case is softer than the first brain phantom without $BaSO_4$ and also softer than the actual brain tissue.

Secondly, the stiffness of the tumor phantom needs to be close to the GBM tissue. The tumor phantom with $BaSO_4$ was too soft, not compact enough and thus fell apart. Reasons for this could be the too high $BaSO_4$ mass fraction, or that $BaSO_4$ does not dissolve enough and therefore the PVA cross-links cannot be formed. Therefore the first tumor, without $BaSO_4$, was used with a stiffness close to the GBM tissue.

Lastly, materials with easily controllable mechanical stiffness were needed for this master project. As can be seen in the range of E values in Table 4.3 that, even with $BaSO_4$, there was a small range between the calculated Young's moduli. However, the $BaSO_4$ did not dissolve, but sank to the bottom of the mould and thereby changed the stiffness. Additionally, the use of $BaSO_4$ did not provide good enough contrast for the CT and the MRI. Consequently, $BaSO_4$ should not be used in future research for the production of PVA phantoms due to the few benefits it offers.

5

Discussion and recommendations

This chapter contains the overall discussion of the master thesis, and provides recommendations for further re search, based on the findings obtained during this research project.

5.1. Discussion

The goal of the discussion is to reflect upon the results, as well as to determine the contribution to the research of this master thesis project. This section consists of three parts. Firstly, the most important results well be discussed. Secondly, it will be discussed whether the requirements for the head phantom have been met. Lastly, the limitations of this project will be discussed.

5.1.1. Most important results
Stiffness of the phantom
Many studies have been done to examine the stiffness of the brain and GBMs tissues using the MRE technique [18][22][34][46][47]. Through the MRE technique the complex shear modulus of the brain and tumors can be examined in a non-invasive way. Also various studies showed that the researchers were capable of producing brain phantoms [18][52][7][13][65]. However, none of these studies showed that they were able to combine the two things, leading to the development of a brain phantom with a stiffness close to the brain.

In this project different PVA samples were made and, with a compression test, the Young's modulus was determined. The complex shear modulus, derived from the MRE data, was converted to an indicative Young's modulus (E^*) and was compared to the E from the compression test. Because of this it was examined which PVA mass fraction, and which number of FT cycles, the PVA sample needed to show the most similar stiffness compared to the actual brain and tumor tissue. Due to these tests it can be better indicated what the desired PVA composition should be. However, the equation used to calculate E^* has only been found in one literature article, and the E^* is only an indication value [60]. More research should be done on this particular topic, in order to compare the MRE data with the compression test. This will be further elaborated upon in section 5.2.2 where the recommendations will be discussed.

Nonetheless, though this thesis project a better indication was found as to which mass fraction is needed to mimic the brain and tumor tissue. A brain phantom with 4,8 wt% PVA, and 2 FT cycles, is very close to the actual brain tissue. Moreover, a tumor phantom with 5,2 wt% and 1 FT cycle is comparable to the GBM tissue. These mass fractions and FT cycles can be used as a guideline for future research and for further development of a brain phantom.

Barium sulfate
For the use case, a brain phantom was needed showing a visible CT and MRI contrast. When preparing a PVA phantom with 1 wt% to 2 wt% $BaSO_4$ shows enough contrast in a CT scan, according to the literature [55][13]. Therefore $BaSO_4$ was added to the brain phantom.

During this project several findings emerged regarding the contrast additive $BaSO_4$. Firstly, the $BaSO_4$ did not dissolve in the PVA solution, and the substance sank to the bottom of the mould. The $BaSO_4$ did show contrast on the CT and MRI scans, but only at the superior part of the brain phantom. Secondly, the $BaSO_4$ did affect the compactness of the PVA. The tumor phantom was produced with 2 wt% $BaSO_4$ but fell apart after production. Lastly, the addition of $BaSO_4$ affected the stiffness of the PVA samples. Using $BaSO_4$ in the PVA samples led to a lower Young's modulus and therefore to a lower stiffness. This must be taken into account for future research. It is not recommended to create a phantom with $BaSO_4$ because of the affects of $BaSO_4$ on the PVA mentioned above.

The use case with the head phantom

There is an increasing interest in the development of brain phantoms to test new medical devices. Because of these brain phantoms medical devices can be tested, evaluated and validated [50][51][52]. In order to develop an accurate brain phantom it is of great importance that the phantom mimics the actual brain tissue as realistically as possible.

During this thesis project a head phantom was needed for an use case for testing a HoMS administration device and a stereotactic frame. Using the head phantom in CT and MRI scans this administration device could be evaluated. The CT scan showed that the tumor was in place before the cannula was inserted into the tumor. Even after insertion of the cannula in the tumor, the tumor phantom was not displaced, which means that the tumor phantom was firmly surrounded by the brain phantom. This could be useful for testing new medical devices which the focus on the insertion in the brain tumor. This is useful for either for medical training purposes or for neurosurgeons in training. The MRI scan showed that when the HoPLLAMS substance was added to the tumor phantom, the tumor fell apart and was subsequently displaced. This should be investigated further in future research with a focus on the injection of the HoPLLAMS substance.

5.1.2. Requirements

In this subsection the head phantom will be evaluated with regard to the requirements. The list of requirements is as follows:

1. The stiffness of the brain phantom must be close to real brain

2. The stiffness of the tumor phantom must be close to GBMs

3. Materials with easily controllable mechanical properties should be used

4. Easy and inexpensive to manufacture

5. No displacement of the tumor phantom in the brain during the production process

6. Contrast for CT/MRI

The first requirement states that the stiffness of the brain phantom needs to be close to the real brain. During this thesis project two brain phantoms were produced. The Young's modulus (E = 8,9 kPa) of the first brain phantom was between the range of the indicative Young's modulus ($E^* = 9,57 \pm 2,03$ kPa). Therefore it can be concluded that creating a brain phantom with 4,8 wt% PVA and 2 FT cycles did meet the first requirement. However, the second brain phantom, produced for the use case did not meet the requirement. due to the addition of $BaSO_4$. Nevertheless, using the mass fraction for the brain phantom without the addition of $BaSO_4$ will result in a brain phantom with a realistic stiffness compared to actual brain tissue.

The second requirement states that the stiffness of the tumor phantom needs to be close to the real GBM tissue. In a tumor phantom, created during this thesis project, the Young's modulus (E = 5,8 kPa) of the tumor phantom was between the range of the indicative Young's modulus ($E^* = 4,93 \pm 1,45$ kPa). The tumor phantom was stiffer compared to the actual GBM tissue. Nonetheless, when a tumor phantom is produced, with 5,2 wt% and 1 FT cycle, this will lead to the conclusion that the second requirement has been met.

The third requirement is that the material used for the production of the brain and tumor phantoms needs to posses easily controllable mechanical properties. PVA was used for the production process, and the stiffness was examined and discussed in subsections 3.2.3 and 4.5.3. The stiffness was easy to control by changing the

mass fraction or by changing the number of FT cycles. Nonetheless, due to the lack of available information about PVA it was more difficult to find the exact mass fraction and number of FT cycles needed to mimic the indicative Young's modulus. Additionally, by adding $BaSO_4$ to the PVA solution the stiffness of the PVA was changed and this would therefore not be recommended in future research. In all it can be concluded that the PVA material had easily controllable mechanical properties despite the lack of information in the literature.

The fourth requirement is that the manufacturing process needs to be inexpensive and easy to do. There is no real cost analysis done on this, as the head phantom in this thesis project is a proof of concept and not a commercial product. However, as discussed in subsection 4.1.3, PVA is an expensive material. Considering that more than one phantom was made during this project, brain phantoms are expensive. Furthermore, the skull phantom and the production of the mould are relatively inexpensive as the materials used for the 3D printing technique are inexpensive. The manufacturing process of the PVA, the mould and the skull was relatively easy to do. However, the mould needs to be improved in order to stop it leaking, thus the brain phantom can potentially be less expensive and also easier to manufacture. Therefore, it cannot be concluded that it is a easy to manufacture a low-cost phantom.

The fifth requirement states that there should not be any displacement of the tumor phantom in the brain, during the production process. At first the tumor phantom did not stay in place. However, after changing the location and the material of the tumor insert, the tumor phantom was more secure in the brain. Correspondingly, the CT images show that the tumor phantom was well enclosed by the brain phantom. Another interesting finding by the CT scan was, that when the cannula was inserted the tumor phantom, no displacement happened. Based on these findings, one can conclude that there was no displacement of the tumor phantom during the production process and that the tumor is well enclosed. Therefore the fifth requirement has been met.

The sixth requirement states that the phantom need to show sufficient contrast for to be used for a CT and MRI scan. In subsection 4.3.3 the contrast of the head phantom was discussed in the CT scan. There was enough contrast to make the brain and tumor phantom visible but not to enough to see an obvious difference between the tumor and the brain phantom. The $BaSO_4$ showed a brighter contrast, but it did not dissolve in the PVA solution. In addition, the skull was minimally visible in the CT scan and needs to be improved by using PLA $CaCO_3$ in future research. The MRI contrast was discussed in subsection 4.4.3. The brain phantom showed great contrast in the MRI scan, and the tumor and brain phantom could be easily distinguished. Again, the skull phantom was not visible in the MRI scan. It could therefore be concluded that the brain and tumor phantom showed enough contrast in the MRI and CT scan, but that the skull phantom did not. Therefore the sixth requirement has been met.

5.1.3. Limitations
Mechanical properties
The focus of this thesis project was on the stiffness of the brain and GBM tumor tissues and to mimic these in a brain phantom. However, comparing the MRE data, found in the literature, with the compression test data gave an indication value and not an exact value. This is due to the limitation of a lack of available information. In order to compare the dynamic MRE tests with the quasi-static compression test a much larger research must be carried out. This was not possible during this research project, due to the limitations in time. Therefore, more research needs to be done on comparing the Young's modulus to the complex shear modulus of the MRE, and this will be elaborated upon in section 5.2. In addition, many more mechanical properties exist than just the stiffness of a material. These properties have not been included into this project and are certainly interesting to look at in future research.

Production process
Since the date of the CT and MRI scan had already been set there were some limitations during the production process, due to the lack of time. Firstly, the mould for the brain phantom was leaking, which caused the phantom to be anatomically incorrect. Therefore the anatomically incorrect phantom was used for the use case. Also the effect of the $BaSO_4$ was examined after the use case. This resulted in the brain phantom that was used for the use case with an incorrect stiffness. This was due to the $BaSO_4$ that was added to the PVA solution to create CT contrast.

5.2. Recommendations

This section contains the recommendations for further research, which are based on the findings obtained during this master thesis project. Five main topics are interesting for follow-up research.

5.2.1. Mechanical properties

This thesis project was mainly focused on the Young's modulus, also called the modulus of elasticity, which measures the stiffness in a material. But there are actually many more mechanical properties that could have been examined in order to create a realistic brain phantom [66]. Even though the brain itself is complex to investigate, more study could have been done on the properties of PVA. For further research it is recommended to include more mechanical properties in the study. This allows for the optimization of the brain phantom and make it more realistic. An other thing that should be studied in future research is the difference in stiffness between the cerebrum, the cerebellum and the gray and white matter.

5.2.2. MRE scan

During this thesis project the stiffness of the phantom was compared to MRE data found in the literature. As mentioned in subsection 5.1.1 more research is needed on comparing these tests with each other. For future research it would be of great interest to make a MRE scan of the brain phantom. Though this the MRE data made of the phantom can be compared to the MRE of the real brain. Hereby a more accurate brain phantom can be created with the right stiffness. Nevertheless, a MRE scan is not available everywhere, and therefore this needs to be planned far in advance.

5.2.3. CT/MRI contrast

The skull phantom was not visible during the CT and MRI scans. To let the skull phantom show contrast in the CT scan, the skull could be printed using the PLA $CaCO_3$ material. However, if the skull needs to be visible for the MRI scan the PLA $CaCO_3$ material will not make any difference. Therefore, the skull should be coated with a glue, or a greasy substance, in order to create more contrast. Another method to improve the MRI contrast is by 3D printing the skull with a photopolymer resin [64]. Also, the contrast agent $BaSO_4$ is not recommended for a PVA sample due to the effect it has on the stiffness and its insolubility.

5.2.4. Production of the mould

The production of the mould needs to be improved in order to not let it leak and thereby creating a more anatomically correct phantom. During this thesis project it was already proven that, after the production of a brain phantom, the mould needs to be re-coated with XTC-3D$^{\text{TM}}$. Furthermore, by adding a large amount of petroleum jelly between the mould parts, and by taping the parts firmly together, this can also partially prevent the mould from leaking. However, the mould should be improved by changing the design. To prevent the mould from leaking a rubber layer between the mould parts should be added. This rubber layer can ensure that the mould parts better fit together. What also can be done is adding a mounting system on the outside of the mould, so that the moulds fit together more tightly. This could be done with a lever lock.

5.2.5. Sensible difference between the tumor and brain

There is a difference in stiffness between the tumor and brain tissue. According to Dr. R.F. Kuiters the difference in stiffness is sensible when a tumor is penetrated by a needle (personal communication, May 03, 2020). This could also be interesting to investigate in order to optimize a brain phantom. When a brain phantom can mimic the same sense that a neurosurgeon feels when penetrating a tumor, it would be a great training method. Through a neurosurgeon in training can practice this by detecting and penetrating the tumor. For future research a brain and a tumor phantom can be created, and tested by neurosurgeons, to evaluate whether there is a sensible difference between the brain and tumor phantom.

<div align="right">

6

</div>

<div align="right">

Conclusion

</div>

In chapter 1, the introduction, the research questions were given. The objective of this thesis project is defined as the development of a brain phantom with a glioblastoma multiforme tumor with a similar stiffness compared to the biological human brain and tumor tissue. The three research questions are answered in this section and the answers will determine whether the research objective has been obtained.

Is it possible to produce a brain phantom with a GBM tumor phantom?

Previous research has shown that a brain phantom can improve neurological training's and therefore the patients outcome. Patients' who suffer from a GBM brain tumor have a low survival rate and therefore the focus of this thesis is to include a GBM tumor phantom into a brain phantom. The results show that it is possible to produce a brain phantom with a GBM tumor phantom.

A PVA brain phantom was made in a patient-specific 3D printed mould of PLA. In the mould a tumor insert was placed that dissolved after the production of the PVA phantom. Through this, a hollow space was left where subsequently a PVA tumor phantom was placed in. The PVA tumor phantom was also made in a 3D printed mould of PLA. Additionally, a patient-specific skull was 3D printed into three parts which enabled the brain to be placed inside the skull.

During an use case a brain phantom was needed and a CT and MRI scan were carried out. Through the CT scan it was seen that the tumor phantom was tightly surrounded by the brain phantom and did not displace when a cannula was inserted.

Nonetheless, there are some improvements needed for the design of the mould of the brain phantom. During this thesis project the mould was leaking, which led to an anatomically incorrect brain phantom. Nevertheless, the phantom was still useful for a use case that was carried out. Through this use case medical devices were tested and evaluated.

This leads to the following conclusion: that the production of a brain phantom with a GBM tumor is possible.

Is it possible to produce a brain phantom with a stiffness comparable to the stiffness found in the literature?

Multiple brain phantoms have been developed in the last couple of years, except for a brain phantom with realistic stiffness compared to the actual brain tissue. Therefore, this master thesis has focused on creating a brain phantom with a stiffness as realistic as possible. The results of this research show that it is possible to create a brain phantom with realistic stiffness.

Several PVA samples were produced and a compression test was carried out. The Young's modulus, derived from the compression test, was compared to the indicative Young's modulus calculated from the complex shear modulus extracted from the literature. Because of this, the mass fraction and FT cycles were found

that had the closest stiffness to actual brain tissue and were therefore suitable for the production of the brain phantom. The PVA samples, with 4,8 wt% PVA and 2 FT cycles, can mimic the stiffness of the brain tissue realistic as possible and can therefore be used for the production of a brain phantom.

For the use case a phantom was created with $BaSO_4$ in order to create CT and MRI contrast. However, the $BaSO_4$ did not dissolve properly, influenced the compactness of the tumor phantom, and changed the stiffness of the PVA samples. In addition, the phantom parts, without the added $BaSO_4$ already had a good visibility and therefore it is not recommended to use $BaSO_4$ in future research.

It can be concluded that using the above mentioned mass fraction will results in a brain phantom with a comparable stiffness to the literature.

Is it possible to produce a GBM tumor phantom with a stiffness comparable to the stiffness found in the literature?

In order to produce a realistic brain phantom with a GBM tumor phantom, the focus was also on creating a tumor phantom with a comparable stiffness to the GBM tissue. Therefore, the stiffness of the Young's modulus of the PVA samples was also compared to the indicative Young's modulus of the GBMs in the literature. Again the sample with the stiffness closest to the GBM tissue was chosen for the production of the tumor phantom. The PVA samples with 5,2 wt% and 1 FT cycle had the closest stiffness compared to the stiffness of the actual GBM tissue.

Based on the results of this thesis project it can be concluded that it is possible to produce a GBM tumor phantom with a comparable stiffness to the GBM stiffness found in the literature.

Taking into account the above mentioned research questions, and their conclusions, one can see that is it possible to develop a brain phantom with a glioblastoma multiforme tumor with a comparable stiffness to the biological human brain and tumor tissues. However, it can not be concluded that these stiffnesses are exactly the same as those of the brain and GBM tissues. Therefore, for follow-up research it would be of great value to carry out a MRE scan of the brain phantom in order to better compare these. Yet, the stiffness of the brain and tumor phantom are very close to the stiffness found in the literature. Therefore, the mass fraction, and the FT cycles, used for the production of the brain and tumor phantom can be used as a guideline for future research.

Bibliography

[1] H Gray. *Gray's anatomy*. 35th ed. Longman group Ltd, 1973.

[2] Michael C Dewan et al. "Global neurosurgery: the current capacity and deficit in the provision of essential neurosurgical care. Executive Summary of the Global Neurosurgery Initiative at the Program in Global Surgery and Social Change". In: *Journal of neurosurgery* 130.4 (2018), pp. 1055–1064.

[3] *Brain Tumor Types & Symptoms - National Brain Tumor Society*. `https://braintumor.org/brain-tumor-information/understanding-brain-tumors/tumor-types/`. Accessed: 16-04-2020.

[4] O Van Tellingen et al. "Overcoming the blood–brain tumor barrier for effective glioblastoma treatment". In: *Drug Resistance Updates* 19 (2015), pp. 1–12.

[5] Yekaterina A Miroshnikova et al. "Tissue mechanics promote IDH1-dependent HIF1α–tenascin C feedback to regulate glioblastoma aggression". In: *Nature cell biology* 18.12 (2016), pp. 1336–1345.

[6] Ryoong Huh et al. "Therapeutic effects of Holmium-166 chitosan complex in rat brain tumor model". In: *Yonsei medical journal* 46.1 (2005), p. 51.

[7] Brian W Pogue and Michael S Patterson. "Review of tissue simulating phantoms for optical spectroscopy, imaging and dosimetry". In: *Journal of biomedical optics* 11.4 (2006), p. 041102.

[8] Zhengchu Tan et al. "Composite hydrogel: A high fidelity soft tissue mimic for surgery". In: *Materials & Design* 160 (2018), pp. 886–894.

[9] Ruth G Nagassa et al. "Advanced 3D printed model of middle cerebral artery aneurysms for neurosurgery simulation". In: *3D printing in medicine* 5.1 (2019), p. 11.

[10] Joshua A Minton, Amin Iravani, and Azizeh-Mitra Yousefi. "Improving the homogeneity of tissue-mimicking cryogel phantoms for medical imaging". In: *Medical physics* 39.11 (2012), pp. 6796–6807.

[11] Adomas Bunevicius et al. "MR elastography of brain tumors". In: *NeuroImage: Clinical* 25 (2020), p. 102109.

[12] Anna-Lisa Kofahl et al. "Combining rheology and MRI: Imaging healthy and tumorous brains based on mechanical properties". In: *Magnetic resonance in medicine* 78.3 (2017), pp. 930–940.

[13] F Kor. "The design of an anthropomorphic head phantom". In: *TU Delft* (2019).

[14] Daniel C Stewart et al. "Mechanical characterization of human brain tumors from patients and comparison to potential surgical phantoms". In: *PLoS One* 12.6 (2017).

[15] Marco Lai et al. "Development of a CT-compatible anthropomorphic skull phantom for surgical planning, training, and simulation". In: *Medical Imaging 2021: Imaging Informatics for Healthcare, Research, and Applications*. Vol. 11601. International Society for Optics and Photonics. 2021, 116010A.

[16] Dana van der Molen. "Literature review of the mechanical properties of the brain and brain tumors". In: *TU Delft* (2020).

[17] J Gordon Betts et al. *Anatomy and Physiology - The Skull*. `https://opentextbc.ca/anatomyandphysiology/chapter/7-1-the-skull/`. Accessed: 16-06-2020. Mar. 2013.

[18] Miriam Navarro-Lozoya et al. "Development of phantom material that resembles compression properties of human brain tissue for training models". In: *Materialia* 8 (2019), p. 100438.

[19] Bruce Fischl and Anders M Dale. "Measuring the thickness of the human cerebral cortex from magnetic resonance images". In: *Proceedings of the National Academy of Sciences* 97.20 (2000), pp. 11050–11055.

[20] Kinaan Javed and Forshing Lui. "Neuroanatomy, Cerebral Cortex". In: *StatPearls [Internet]*. StatPearls Publishing, 2019.

[21] S Budday et al. "Towards microstructure-informed material models for human brain tissue". In: *Acta Biomaterialia* 104 (2020), pp. 53–65.

[22] Bruno Mota et al. "White matter volume and white/gray matter ratio in mammalian species as a conse-
      quence of the universal scaling of cortical folding". In: *Proceedings of the National Academy of Sciences*
      116.30 (2019), pp. 15253–15261.

[23] *Difference between white and gray matter.* `https://difference.guru/difference-between-`
      `white-and-gray-matter/`. Accessed: 17-06-2020. Feb. 2018.

[24] Elaine Nicpon Marieb and Katja Hoehn. *Human anatomy & physiology.* Pearson education, 2007.

[25] Karol Miller et al. "Biomechanical modeling and computer simulation of the brain during neurosurgery".
      In: *International journal for numerical methods in biomedical engineering* 35.10 (2019), e3250.

[26] T-Y Jung et al. "Application of neuronavigation system to brain tumor surgery with clinical experience
      of 420 cases". In: *min-Minimally Invasive Neurosurgery* 49.04 (2006), pp. 210–215.

[27] Huile Gao and Xinguo Jiang. "Progress on the diagnosis and evaluation of brain tumors". In: *Cancer
      Imaging* 13.4 (2013), p. 466.

[28] Charles W Schmidt. *CT scans: balancing health risks and medical benefits.* 2012.

[29] *Computed Tomography (CT) - National Institute of Biomedical Imaging and Bioengineering.* `https:`
      `//www.nibib.nih.gov/science-education/science-topics/computed-tomography-ct`.
      Accessed: 15-06-2020.

[30] Stephen P Power et al. "Computed tomography and patient risk: facts, perceptions and uncertainties".
      In: *World journal of radiology* 8.12 (2016), p. 902.

[31] Katie L McMahon, Gary Cowin, and Graham Galloway. "Magnetic resonance imaging: the underlying
      principles". In: *journal of orthopaedic & sports physical therapy* 41.11 (2011), pp. 806–819.

[32] Lynne E Bilston. "Brain tissue mechanical properties". In: *Biomechanics of the Brain.* Springer, 2011,
      pp. 69–89.

[33] Uulke A van der Heide et al. "MRI basics for radiation oncologists". In: *Clinical and translational radi-
      ation oncology* 18 (2019), pp. 74–79.

[34] John Zhang et al. "Viscoelastic properties of human cerebellum using magnetic resonance elastogra-
      phy". In: *Journal of biomechanics* 44.10 (2011), pp. 1909–1913.

[35] A Franck and TA Instruments Germany. "Viscoelasticity and dynamic mechanical testing". In: *TA In-
      struments, New Castle, DE, USA AN004* (1993).

[36] M Simon et al. "Non-invasive characterization of intracranial tumors by magnetic resonance elastog-
      raphy". In: *New Journal of Physics* 15.8 (2013), p. 085024.

[37] Kay M Pepin et al. "MR elastography analysis of glioma stiffness and IDH1-mutation status". In: *Amer-
      ican Journal of Neuroradiology* 39.1 (2018), pp. 31–36.

[38] *Brain Tumors - AANS.* `https://www.aans.org/en/Patients/Neurosurgical-Conditions-and-`
      `Treatments/Brain-Tumors`. Accessed: 16-04-2020.

[39] Federico Pessina et al. "Outcome evaluation of oligometastatic patients treated with surgical resection
      followed by hypofractionated stereotactic radiosurgery (HSRS) on the tumor bed, for single, large brain
      metastases". In: *PloS one* 11.6 (2016).

[40] Allen Perkins and Gerald Liu. "Primary brain tumors in adults: diagnosis and treatment". In: *American
      family physician* 93.3 (2016), pp. 211–217.

[41] Sreenivasa R Chandana et al. "Primary brain tumors in adults". In: *American family physician* 77.10
      (2008), p. 1423.

[42] Benjamin D Fox et al. "Epidemiology of metastatic brain tumors". In: *Neurosurgery Clinics* 22.1 (2011),
      pp. 1–6.

[43] Jan C Buckner et al. "Central nervous system tumors". In: *Mayo Clinic Proceedings.* Vol. 82. 10. Elsevier.
      2007, pp. 1271–1286.

[44] Frank H Netter. *The CIBA collection of medical illustrations.* Vol. 1. CIBA Pharmaceutical products, 1948.

[45] Suvi Larjavaara et al. "Incidence of gliomas by anatomic location". In: *Neuro-oncology* 9.3 (2007), pp. 319–
      325.

[46] GT Fallenstein, Verne D Hulce, and John W Melvin. "Dynamic mechanical properties of human brain tissue". In: (1969).

[47] Karol Miller and Kiyoyuki Chinzei. "Mechanical properties of brain tissue in tension". In: *Journal of biomechanics* 35.4 (2002), pp. 483–490.

[48] *New treatment of brain tumors in dogs: minimally invasive image-guided treatment by injection of radioactive holmium-166 microspheres.* `https://www.uu.nl/en/organisation/veterinary-service-and-cooperation/new-treatment-of-brain-tumors-in-dogs`. Accessed: 01-06-2021. Oct. 2020.

[49] Martijn de Vries. "Development of a holmium microshere administration device for treatment of brain malignancies". In: *TU Delft* (Nov. 2018).

[50] Madhuvanthi A Kandadai, Jason L Raymond, and George J Shaw. "Comparison of electrical conductivities of various brain phantom gels: Developing a 'brain gel model'". In: *Materials Science and Engineering: C* 32.8 (2012), pp. 2664–2667.

[51] Hussein Girnary. "Brain Phantom Project". In: (2007).

[52] Alexander Leibinger et al. "Soft tissue phantoms for realistic needle insertion: a comparative study". In: *Annals of biomedical engineering* 44.8 (2016), pp. 2442–2452.

[53] KJM Surry et al. "Poly (vinyl alcohol) cryogel phantoms for use in ultrasound and MR imaging". In: *Physics in Medicine & Biology* 49.24 (2004), p. 5529.

[54] Shan Jiang, Sha Liu, and Wenhao Feng. "PVA hydrogel properties for biomedical application". In: *Journal of the mechanical behavior of biomedical materials* 4.7 (2011), pp. 1228–1233.

[55] Sean Jy-Shyang Chen et al. "An anthropomorphic polyvinyl alcohol brain phantom based on Colin27 for use in multimodal imaging". In: *Medical physics* 39.1 (2012), pp. 554–561.

[56] José M Martınez and Boguslaw J Jarosz. "3D perfused brain phantom for interstitial ultrasound thermal therapy and imaging: design, construction and characterization". In: *Physics in Medicine & Biology* 60.5 (2015), p. 1879.

[57] Jason S Naftulin, Eyal Y Kimchi, and Sydney S Cash. "Streamlined, inexpensive 3D printing of the brain and skull". In: *PloS one* 10.8 (2015), e0136198.

[58] *Fused deposition modeling (FDM) 3D Printers.* `https://www.3dinthebox.eu/nl/3d-printers/fdm-3d-printers/`. Accessed: 21-05-2021.

[59] Milovan Regodic, Zoltan Bardosi, and Wolfgang Freysinger. "Automated fiducial marker detection and localization in volumetric computed tomography images: a three-step hybrid approach with deep learning". In: *Journal of Medical Imaging* 8.2 (2021), p. 025002.

[60] F Morin et al. *Biomechanical modeling of brain soft tissues for medical applications. Biomechanics of living organs.* 2017.

[61] *Ultimaker Filament PLA - PVA.* `https://www.makerpoint.nl/nl-nl/3d-printing/consumables/filament/ultimaker/material-grade=pla,pva/`. Accessed: 21-05-2021.

[62] *XTC-3D ^{TM}, High Performance 3D Print Coating / Smooth-On, Inc.* `https://www.smooth-on.com/product-line/xtc-3d/`. Accessed: 19-05-2021.

[63] *Poly(vinyl alcohol) Mw 89,000 - 98,000, 99% + hydrolyzed / Sigma Aldrich.* `https://www.sigmaaldrich.com/`. Accessed: 10-06-2021.

[64] Robba Rai et al. "3D printed phantoms mimicking cortical bone for the assessment of ultrashort echo time magnetic resonance imaging". In: *Medical physics* 45.2 (2018), pp. 758–766.

[65] Roland K Chen and AJ Shih. "Multi-modality gellan gum-based tissue-mimicking phantom with targeted mechanical, electrical, and thermal properties". In: *Physics in Medicine & Biology* 58.16 (2013), p. 5511.

[66] Joshua Pelleg. *Mechanical properties of materials.* Vol. 190. Springer Science & Business Media, 2012.

Appendices

A

Stress-strain curves of the 7 PVA samples

In this Appendix extra stress-strain curves are provided of each sample group and their stress-strain curves.
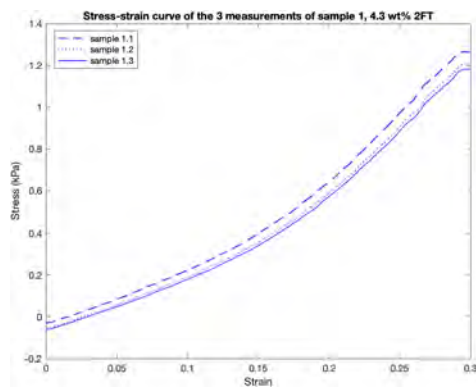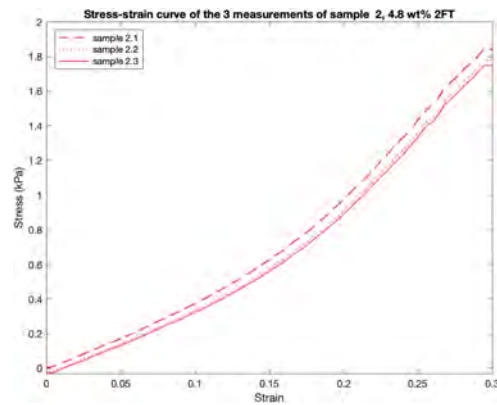

Figure A.1: The stress-strain curves of sample group 1
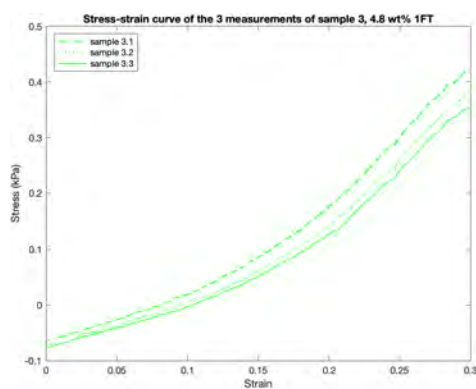

Figure A.2: The stress-strain curves of sample group 2
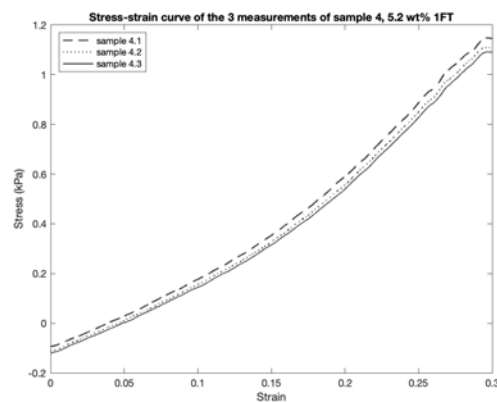

Figure A.3: The stress-strain curves of sample group 3

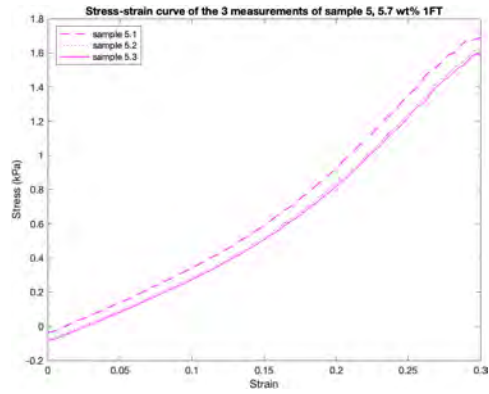**Figure A.4:** The stress-strain curves of sample group 4

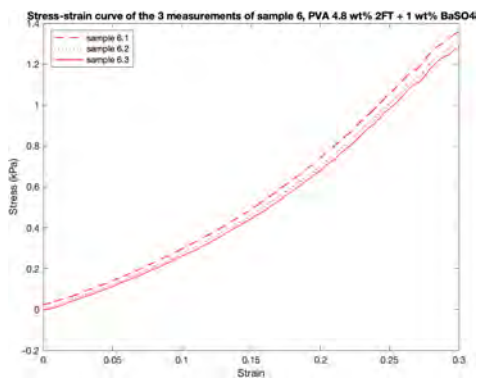**Figure A.5:** The stress-strain curves of sample group 5

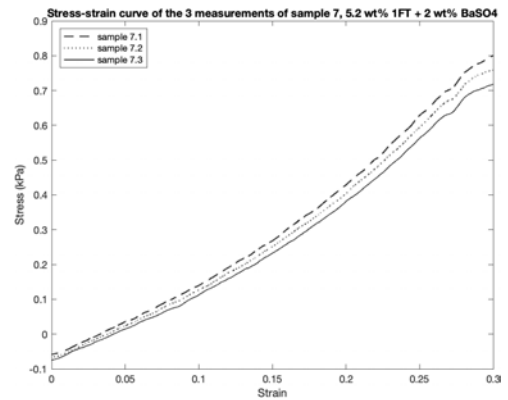**Figure A.6:** The stress-strain curves of sample group 6 + BaSO$_4$

Figure A.7: The stress-strain curves of sample group 7 + BaSO$_4$

B

Production of PVA

In this appendix the production of PVA is described step by step.

STEP I
The PVA powder, coolant, distilled water (and barium sulfate) need to be weight according to the recipe.

STEP II
The materials need to be added together in a beaker. In order to dissolve the PVA powder, the mixture needs to be heated till 93 °C and stirred continuously. Cover up the top of the beaker to prevent the water from evaporating.

STEP III
When all PVA powders are dissolved the PVA solution can be removed from the heating plate. Let it cool down for some time (1 or 2 hours) and then pour the solution in the mould.

STEP IV
Place the mould with the PVA solution in a freezer for 24 hours. The freezer needs to be at - 25 °.

STEP V
After the 24 hours in the freezer the mould needs to set to rest at room temperature for a few hours.

STEP VI
When the mould is at room temperature the mould can be removed and the phantom is ready to use.

Note 1. When a phantom with more then 1 freeze thaw is needed, step IV and V must be repeated.
Note 2. The phantom can be stored in a container with distilled water in the refrigerator for a year.

C

Printed files and settings

3D print	Material	Thickness (mm)	Infill (%)	Support	Color	Date	Printer
Mould brain top	PLA	0.2	40	PVA	Metallic	03-12-20	Ultimaker 3E
Mould brain bottom P1	PLA	0.2	40	PVA	Metallic	04-12-20	Ultimaker 3E
Mould brain bottom P2	PLA	0.2	40	PVA	Metallic	04-12-20	Ultimaker 3E
Tumor insert	PLA	0.15	40	PVA	Metallic	18-01-21	Ultimaker 3E
Mould tumor bottom	PLA	0.15	40	PVA	Metallic	25-01-21	Ultimaker 3E
Mould tumor top	PLA	0.15	40	PVA	Metallic	25-01-21	Ultimaker 3E
Tumor insert (2)	PVA	0.15	40	PVA	Clear	19-02-21	Ultimaker 3E
Mould brain bottom P2 (2)	PLA	0.2	40	PVA	White	22-02-21	Ultimaker 3E
Jaw	PLA CaCO$_3$	0.15	30	PVA	White	23-02-21	Ultimaker 3
Skull middle	PLA CaCO$_3$	0.15	30	PVA	White	27-02-21	Ultimaker 3E
Skull middle	PLA	0.15	30	PVA	White	27-02-21	Ultimaker 5
Skull top	PLA	0.15	30	PVA	White	27-02-21	Ultimaker 5
Jaw	PLA	0.15	30	PVA	White	03-03-21	Ultimaker 3E
Note. The 3D printers are located at the Robotlab at 3mE							

D

Exact sizes of the 3D structures

In this appendix the sizes the 3D structures are listed. These sizes are partly extracted from the thesis by F. Kor [13].

Pins for the brain mould

	Specification	**Dimensions (mm)**
Cone bottom	Bottom diameter	5
	Top diameter	3
	Height	5
Cone hole	Bottom diameter	5,4
	Top diameter	3,4
	Height	5,4

Table D.1: The sizes of the pins on the brain mould

Pins for the tumor mould

	Specification	**Dimensions (mm)**
Cone bottom	Bottom diameter	3
	Top diameter	2
	Height	4
Cone hole	Bottom diameter	3,4
	Top diameter	2,4
	Height	4,4

Table D.2: The sizes of the pins on the tumor mould

Tumor insert sizes

	Specification	**Dimensions (mm)**
Ball	Radius	16
Rod	Length from centre	70
	Diameter	8

Table D.3: The sizes of the tumor insert

Pins for the skull

	Specification	Dimensions (mm)
Cone bottom	Bottom diameter	3,5
	Top diameter	2,5
	Height	4
Cone hole	Bottom diameter	3,8
	Top diameter	2,8
	Height	4,3

Table D.4: The sizes of the pins on the skull phantom

E

Extra figures of the head phantom

In this appendix some extra figures are included of the head phantom.

Figure E.1: The tore in the brain phantom and tumor in it

Figure E.2: Tumor phantoms with $BaSO_4$

Figure E.3: Brain phantom in the skull

F

MRI and CT images

CT scans of the brain phantom in sagittal plane before the injection
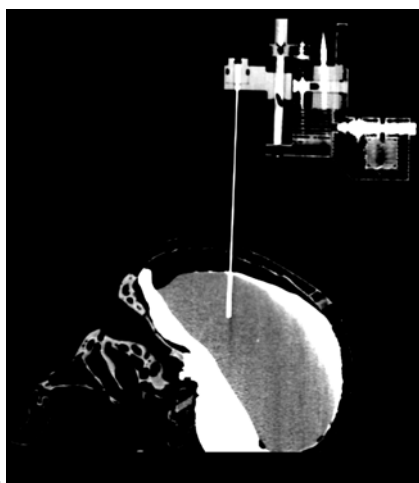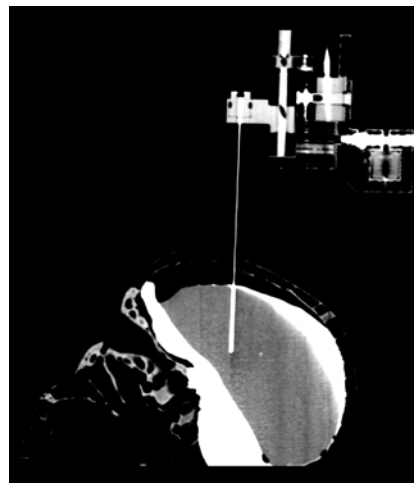

Figure F.1: CT4 the cannula at the edge of the tumor

Figure F.2: CT5, the cannula at $\frac{2}{3}$ of the tumor

CT scans of the brain phantom in sagittal plane during the two injection rounds
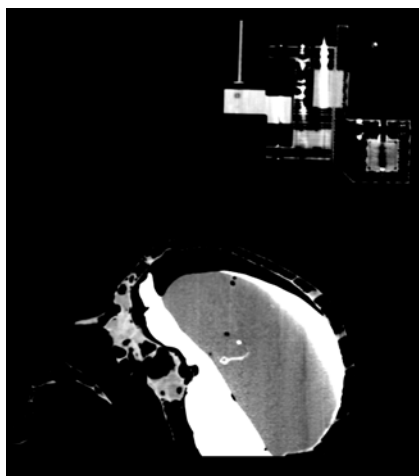
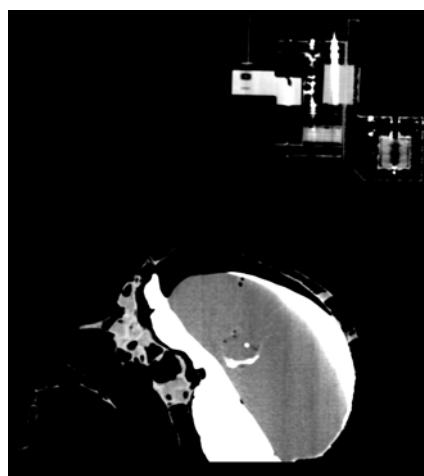Figure F.3: CT6, after the first injection round

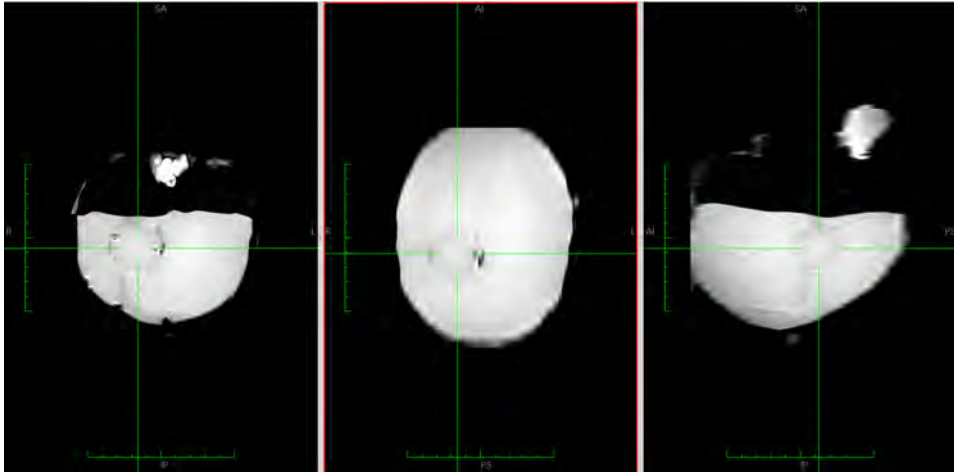Figure F.4: CT8, after the second injection round

MRI scan before the injection

Figure F.5: MRI1 before the injection
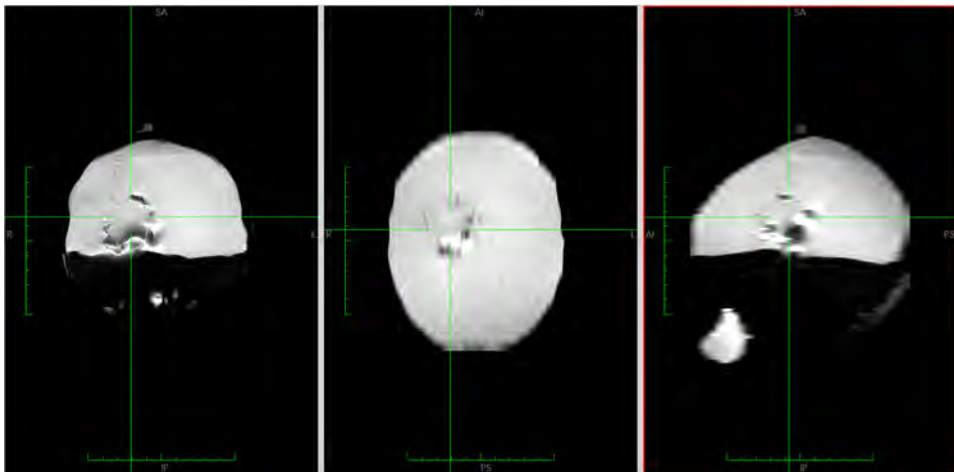
MRI after the injection

Figure F.6: MRI1 after the injection